Nature. Author manuscript; available in PMC 2019 March 26.

Published in final edited form as:
Nature. 2018 October ; 562(7726): 223–228. doi:10.1038/s41586-018-0552-x.

Erythro-myeloid progenitors contribute endothelial cells to blood vessels

Alice Plein[#1], **Alessandro Fantin**[#1], **Laura Denti**[1], **Jeffrey W. Pollard**[2], and **Christiana Ruhrberg**[1,^]

[1]UCL Institute of Ophthalmology, University College London, 11-43 Bath Street, London EC1V 9EL, UK

[2]MRC Centre for Reproductive Health, University of Edinburgh, 47 Little France Crescent, Edinburgh EH16 4TJ, UK

[#] These authors contributed equally to this work.

Abstract

The earliest blood vessels in the mammalian embryo are formed when endothelial cells (ECs) differentiate from angioblasts and coalesce into tubular networks. Thereafter, the endothelium is thought to expand solely by proliferation of pre-existing ECs. Here we show that the earliest precursors of erythrocytes, megakaryocytes and macrophages, the yolk sac-derived erythro-myeloid progenitors (EMPs), provide a complementary source of ECs that are recruited into pre-existing vasculature. Whereas a first wave of yolk sac-resident EMPs contributes ECs to the yolk sac endothelium, a second wave of EMPs colonises the embryo and contributes ECs to intraembryonic endothelium in multiple organs, where they persist into adulthood. By demonstrating that EMPs constitute a hitherto unrecognised source of ECs, we reveal that embryonic blood vascular endothelium expands in a dual mechanism that involves both the proliferation of pre-existing ECs and the incorporation of ECs derived from hematopoietic precursors.

Blood vessels distribute oxygen, nutrients, hormones and immune cells through the vertebrate body and help remove waste molecules. Accordingly, functional blood vessel formation during embryogenesis is a prerequisite for vertebrate life. Endothelial cells (ECs) form the inner lining of blood vessels; they first arise from mesenchymal precursors termed

[^]Correspondence and requests for materials should be addressed to Professor Christiana Ruhrberg, Tel.: 44 (0)20 7608 4017; c.ruhrberg@ucl.ac.uk.

Author contributions

A.P., A.F. and C.R. conceived and planned this study, analysed data and co-wrote the manuscript. L.D. performed genetic crosses and genotyping. A.P. and A.F. performed experiments either together or replicated each other's experiments, except for the cell cycle and *Hoxa* studies, which were carried out by A.P and A.F., respectively. J.W.P. provided mouse strains. C.R. supervised the project. All authors reviewed and edited the manuscript.

Author information. Reprints and permission information is available at www.nature.com/reprints.

The authors declare no competing interests.

Data availability. All sequence data used in this study have been deposited in the NCBI Gene Expression Omnibus database (accession number GSE117978) and are listed in Source Data Fig. 6.

Europe PMC Funders Author Manuscripts

angioblasts on embryonic day (E) 7.0 in mice 1. After condensing into yolk sac vasculature and the paired dorsal aortae, ECs proliferate within existing endothelium to increase vascular diameter, sprout into avascular tissue areas or remodel into smaller vessels by intussusceptive growth 1. Current consensus is therefore that embryonic ECs are a self-contained cell lineage that expands without contribution from new angioblasts or circulating precursors. In contrast, circulating endothelial progenitors have been proposed to exist in the adult, although their relationship to myeloid cells (MCs) remains controversial 2.

In addition to their primary roles in the innate immune system, MCs such as monocytes and macrophages also modulate vascular growth 3. For example, the tissue-resident macrophages of the embryonic mouse brain, termed microglia, contact ECs at the tip of neighbouring vessel sprouts to promote their anastomosis into perfused vessel loops 4. In contrast, a direct contribution of MCs to embryonic vascular endothelium has not been reported; thus, genetic lineage tracing with the myeloid *Vav* or *Lyz2* (*Lysm*) promoters does not mark embryonic blood vascular endothelium in mice 5, 6.

Most tissue-resident macrophages arise from erythro-myeloid progenitors (EMPs) that form in the extra-embryonic yolk sac during embryogenesis and also serve as precursors for erythrocytes and megakaryocytes 7–11. In mice, an early EMP wave, also referred to as primitive hematopoietic progenitors, buds from yolk sac endothelium between E7.0 and E8.25 and differentiates by E9.0 into yolk sac macrophages without monocytic intermediates 7, 10, 12–14. These macrophages colonise the embryo proper to generate tissue-resident macrophages, such as microglia in the brain or Langerhans cells in the epidermis 13. A later EMP wave buds from yolk sac endothelium from E8.25 onwards and colonises the liver after the embryonic circulation is established 7, 8, 11, 14, 15. These later-born EMPs expand in the liver into monocytes that subsequently differentiate into tissue-resident macrophages in many organs but not the brain 7, 13.

Lineage tracing with *Csf1r-iCre* identifies ECs in developing brain vasculature

To target early EMPs 7, 10, 12, microglia 16, 17 and other differentiated MCs 18, we and others have used a transgene that expresses CRE recombinase under the promoter for the myeloid lineage gene *Csf1r* (*Fms*), which encodes the colony-stimulating factor 1 receptor, CSF1R. Microglia appear as single YFP^+ cells in hindbrains from *Csf1r-iCre* mouse embryos carrying the $Rosa^{Yfp}$ recombination reporter, with microglia and ECs also stained for isolectin B4 (IB4) (Fig. 1a) 16. As previously shown 4, the number of $IB4^+$ YFP^+ microglia peaked in the hindbrain subventricular zone at E11.5, when vessels fuse into the subventricular vascular plexus (SVP) (Fig. 1b). Surprisingly, we also observed sporadic, elongated $IB4^+$ YFP^+ cells that appeared bound into the endothelium and increased steadily during SVP expansion (Fig. 1a-c; Extended Data Fig. 1a). *Csf1r-iCre*-targeting of vessel-bound cells was not an artefact caused by spontaneous $Rosa^{Yfp}$ recombination or unspecific immunostaining, because littermates lacking *Csf1r-iCre* lacked YFP staining (Fig. 1a). Furthermore, imaging of *Csf1r-iCre* hindbrains carrying *CAG-Cat-Egfp* or $Rosa^{tdTom}$ as alternative recombination reporters confirmed targeting of both microglia and vessel-bound

elongated cells (Extended Data Fig. 1b,c). The tamoxifen-induced activation of CRE expressed from an independently generated *Csf1r-Mer-iCre-Mer* transgene that also targets MCs 19 similarly targeted vessel-bound cells in addition to microglia (Fig. 1d). Corroborating the endothelial identify of *Csf1r-iCre*-targeted vessel-bound cells, they expressed the EC markers ERG and PECAM1, had a similar morphology to ECs targeted with the endothelial-specific *Cdh5-Cre^{ERT2}* transgene, formed junctions with neighbouring ECs via the endothelial cadherin CDH5 and lacked both myeloid and pericyte markers (Fig. 1e, Extended Data Fig. 1d-f).

Csf1r-iCre-mediated EC targeting was not explained by *Csf1r* expression of brain ECs, because hindbrain ECs, unlike microglia, lacked expression of a *Csf1r-Egfp* transgene that faithfully reports *Csf1r* promoter activity 20, 21 and accordingly did not contain CSF1R protein (Extended Data Fig. 2a,b). Moreover, the analysis of published transcriptomic datasets 22 showed that *Csf1r* is not expressed in ECs from embryonic brain, liver or lung, and RT-qPCR analysis of tdTom$^+$ ECs isolated by fluorescence-activated cell sorting (FACS) confirmed that they expressed *Cdh5,* but not *Csf1r* or the myeloid gene *Spi1*, which encodes the PU.1 transcription factor (Extended Data Fig. 2c-g). The lack of endothelial *Csf1r* expression suggests that *Csf1r-iCre*-targeted brain ECs arise from precursors that activate *Csf1r* prior to their incorporation into hindbrain vasculature. These precursors cannot be differentiated MCs such as microglia, whose formation is PU.1-dependent 4, because PU.1 deficiency did not reduce the number of *Csf1r-iCre*-targeted ECs in the E11.5 hindbrain (Fig. 1f-h) or postnatal day (P) 0 striatum (Extended Data Fig. 2h). We therefore investigated whether *Csf1r-iCre*-targeted ECs are derived from PU.1-independent, *Csf1r*-expressing precursors.

Csf1r-iCre-targeted ECs and EMPs share PU.1-independent spatiotemporal origins

As EMPs are PU.1-independent 23, we investigated whether the formation of *Csf1r-iCre*-targeted ECs is spatiotemporally linked to the emergence of *Csf1r*-expressing EMPs from yolk sac hemogenic endothelium, which was visualised by staining for the EC marker VEGFR2. E8.5 *Csf1r-Egfp* yolk sacs contained clusters of round EGFP$^+$ VEGFR2$^+$ cells that protruded from endothelium into the vascular lumen (Fig. 2a), consistent with prior work showing that FACS-isolated EMPs express both *Csf1r* 7 and *Vegfr2* 9, and that EMPs bud from yolk sac endothelium 11. *Csf1r-iCre* lineage tracing in E8.5 yolk sacs similarly identified YFP$^+$ round cells that protruded into the vascular lumen, were VEGFR2$^+$, persisted in PU.1-deficient yolk sacs and expressed the EMP marker KIT 7 (Fig. 2b,c; Extended Data Fig. 3a,b). Even though EGFP expression could not be detected in *Csf1r-Egfp* yolk sac endothelium (Fig. 2a), *Csf1r-iCre;Rosa^{Yfp}* also targeted a subset of yolk sac ECs that lacked obvious KIT expression (Extended Data Fig. 3b), excluding that they were hemogenic ECs 24. Similar to *Csf1r-iCre*-targeted hindbrain ECs, the lineage-traced yolk sac ECs were PU.1-independent (Fig. 2b,c).

The finding that EMP formation correlates with the emergence of *Csf1r-iCre*-targeted yolk sac ECs was corroborated by temporally restricted *Csf1r-Mer-iCre-Mer*-mediated lineage

tracing. As tamoxifen-induced, CRE-mediated reporter recombination peaks approximately 6 h and ends 24 h after tamoxifen injection 25, we activated *Csf1r-Mer-iCre-Mer;Rosa*^{tdTom} in discrete temporal windows by single injections at E8.5, E9.5 or E10.5 before identifying lineage-traced cells in E12.5 yolk sacs (Extended Data Fig. 3c). Inductions at all three stages labelled yolk sac macrophages (Extended Data Fig. 3d), consistent with their origin from *Csf1r*-expressing EMPs 7 and their maintenance of *Csf1r* expression 10, 12. Additionally, E8.5 or E9.5 induction yielded tdTom$^+$ ECs, whereas E10.5 induction did not (Extended Data Fig. 3d). As EMPs are present in the yolk sac at E8.5 and E9.5, but home to the liver thereafter 13, their local availability makes them plausible precursors of *Csf1r-iCre*-labelled yolk sac ECs. In agreement, tamoxifen induction of a *Kit*^{CreERT2} knockin allele at E8.5, when KIT$^+$ early EMPs are still present in the yolk sac 7, lineage-traced both yolk sac ECs and macrophages (Extended Data Fig. 3e,f).

In contrast to early wave EMPs that remain in the yolk sac, the late wave EMPs that populate the embryo are reported to lack *Csf1r* expression, at least when they form in the yolk sac 7. We therefore investigated whether late wave EMPs begin to express *Csf1r* after liver homing and if they are the precursors of *Csf1r*-targeted ECs that appear in the hindbrain from E10.5 onwards. Thus, we combined the *Csf1r-Egfp* expression reporter with *Csf1r-Mer-iCre-Mer;Rosa*^{tdTom} and induced CRE-mediated recombination at E10.5; 24 h later, we FACS-separated the differentiated MCs from EMPs and EMP-derived myeloid progenitors (MPs) 7 from liver and blood (Fig. 3a,b). The differentiated MC populations from both sources contained tdTom$^+$ EGFP$^+$ cells, as expected, but notably, tdTom$^+$ EGFP$^+$ cells were also present in the EMP/MP populations of both liver and blood (Fig. 3a,b; Extended Data Fig. 3g-i). These findings suggest that a subset of intraembryonic EMPs expresses *Csf1r* and can access organs such as the hindbrain via the circulation.

To determine whether the intraembryonic presence of *Csf1r*-expressing late wave EMPs correlated with the emergence of *Csf1r-iCre*-targeted hindbrain ECs, we visualised tdTom expression in E12.5 *Csf1r-Mer-iCre-Mer;Rosa*^{tdTom} hindbrains after E8.5, E9.5 and E10.5 tamoxifen induction (Fig. 3c). The hindbrain vasculature contained tdTom$^+$ ECs following induction at E10.5, but not E8.5 or E9.5, even though the *Csf1r*-expressing microglia were targeted at all stages (Fig. 3d). *Kit*^{CreERT2} induction at E8.5 also caused microglia targeting (Fig. 3e,f), agreeing with microglia arising from yolk sac macrophages generated around E8.5 from KIT$^+$ early wave EMPs 7. *Kit*^{CreERT2} induction at E8.5, when late wave EMPs begin to arise in the yolk sac 7, also yielded tdTom$^+$ ECs in the E12.5 hindbrain (Fig. 3e,f), corroborating that yolk sac-born EMPs can give rise to intraembryonic ECs. Lineage tracing from three independent *Cre* alleles therefore suggests that EMPs give rise to both yolk sac and hindbrain ECs.

The *Csf1r-iCre*-targeted EMP lineage gives rise to ECs *in vitro*

The myeloid and erythroid potential of EMPs has been demonstrated through *in vitro* differentiation 11, 26. Using similar assays, we compared the endothelial potential of FACS-isolated differentiated MC and EMP/MP populations from E12.5 *Csf1r-iCre;Rosa*^{tdTom} liver and blood whilst ensuring that we were excluding contamination by PECAM1$^+$ ECs (Fig. 4a,b). Both cell populations were mostly tdTom$^+$ (Fig. 4c,d). As expected 7, the EMP-

containing population was comprised of round cells with a large nucleus and little cytoplasm, whereas the MC population contained granulocytes, in addition to monocytes in the liver and macrophages in the blood (Fig. 4c,d) For culture, we used methocult to promote the formation of hematopoietic colonies, but included a fibronectin (FN) substrate to facilitate EC differentiation. Differentiated MCs persisted in these cultures as single round/amoeboid cells (Fig. 4e,f) that were tdTom^{+} ERG^{lo} VEGFR2^{lo} (Fig. 4g,h; antibody controls in Extended Data Fig. 4a,b). In contrast, both liver and blood EMPs formed myeloid and erythroid cell colonies in suspension (Fig. 4e,f) and additionally gave rise to single adherent cells that appeared spindle-shaped, were tdTom^{+} ERG^{hi} VEGFR2^{hi} and lacked myeloid cell markers, consistent with an EC identity (Fig. 4g,h; Extended Data Fig. 4c). Together, these experiments demonstrate that EMPs have endothelial potential alongside their known hematopoietic capacity.

Csf1r-iCre-targeted ECs support the growth of embryonic brain vasculature

Hoxa cluster genes modulate haematopoiesis 27 and are upregulated in postnatal compared to adult ECs 28, with HOXA9 also promoting EC differentiation from progenitors in adult ischemic disease 29. Our analysis of published transcriptomic data 9, 30 revealed that *Hoxa* transcripts are enriched in E10.25 compared to E9.0 EMPs or macrophages (Fig. 5a). To investigate whether *Hoxa*-deficiency impairs the formation of EMP-derived hindbrain ECs, we combined *Csf1r-iCre* with a conditional null *Hoxa* cluster mutation (*Hoxa^{fl}*) (Extended Data Fig. 5a). Gene copy analysis showed effective gene targeting in KIT^{+} cells from E12.5 *Csf1r-iCre;Hoxa$^{fl/fl}$* mutant compared to control livers, but the number of CD45^{+} cells, including differentiated MCs, was not reduced (Extended Data Fig. 5b-f). *Hoxa* genes are therefore dispensable for MC specification from late wave EMPs. In contrast, significantly fewer tdTom^{+} ECs, also derived from late wave EMPs, had formed in *Rosa^{tdTom}*-carrying *Csf1r-iCre;Hoxa$^{fl/fl}$* mutant compared to control hindbrains; moreover, SVP complexity was significantly reduced in mutant hindbrains (Fig. 5b-d). Although we observed 20% fewer microglia in mutant compared to control hindbrains (Extended Data Fig. 5g-i), this unlikely contributed to the vascular defect, because even a 50% microglia reduction in *Csf1$^{op/+}$* mutants did not reduce SVP complexity (Extended Data Fig. 5j-l). Together, these findings suggest that *Hoxa* cluster genes promote the formation of EMP-derived brain ECs, which in turn support normal brain vascular development.

EMP-derived ECs have a core endothelial transcriptional signature and preferentially contribute to liver vasculature

Csf1r-iCre-targeted ECs not only appeared morphologically similar to neighbouring ECs (Fig. 1), but also had similarly slow proliferation and overall cell cycle kinetics (Extended Data Fig. 6). Moreover, RNA-Seq analysis of FACS-isolated tdTom^{+} and tdTom^{-} ECs from E12.5 *Csf1r-iCre;Rosa^{tdTom}* embryos showed that they had largely similar transcriptomes, with only few differentially expressed genes, including the expected difference in the *tdTomato* transcript (Fig. 6a-c; Extended Data Fig. 7a). Corroborating their endothelial identity, tdTom^{+} ECs lacked markers for differentiated MCs and other non-EC lineages, but expressed core EC transcripts at similar levels to tdTom^{-} ECs (Fig. 6d,e). Amongst the

differentially expressed genes, markers typical of EC specialisation were under-represented in tdTom$^+$ ECs, such as ephrins and EPH receptors regulating arteriovenous differentiation (Fig. 6e). This observation agrees with *Csf1r-iCre*-targeted ECs being derived from progenitors that are recruited into preformed vascular endothelium. Whereas brain EC markers (e.g. *Slc2a1*) were under-represented in the embryo-wide tdTom$^+$ EC population, liver EC markers were over-represented (e.g. *Oit3, Mrc1*), including early markers of liver sinusoidal differentiation (*Stab2, Lyve1*) 31 (Fig. 6c,f; Extended Data Fig. 7b,c). Similar expression of *Oit3* and *Mrc1* in tdTom$^+$ and tdTom$^-$ liver ECs (Extended Data Fig. 7d) suggests that the over-representation of liver EC transcripts in the total embryonic tdTom$^+$ EC population reflects their preferential contribution to liver vasculature. Immunostaining and FACS of *Csf1r-iCre;Rosa*^{tdTom} E12.5 and E18.5 embryos confirmed that tdTom$^+$ ECs were more prevalent in liver endothelium than tdTom$^-$ ECs (Fig. 6g,i; Extended Data Figs. 8 and 9a,b). As liver EC specialisation markers were present in both tdTom$^-$ and tdTom$^+$ liver ECs at E12.5 (Fig. 6g; Extended Data Fig. 8a), liver ECs of two distinct origins appear to undergo similar organ-specific EC differentiation.

Csf1r-iCre-targeted ECs populate multiple embryonic organs and persist into adulthood

Immunostaining and FACS analyses at E12.5 and E18.5 showed that *Csf1r-iCre*-targeted ECs were also present in heart and lung vasculature at similar levels to the brain (Fig. 6i; Extended Data Figs. 8 and 9a,b). Corresponding immunostaining and FACS analyses showed that tdTom$^+$ ECs persisted in the brain, heart, lung and liver of adults and continued to dominate the adult liver sinusoidal endothelium (Fig. 6h,j; Extended Data Figs. 9c and 10a). Accordingly, all adult organs examined contained EMP-derived ECs.

Discussion

The heterogeneous origin of blood vascular mural cells from distinct populations of mesodermal progenitors, hematopoietic and neural crest cells is established 32. Here, we show that embryonic vascular endothelium has two major origins. Thus, ECs emerge via a classical pathway of angioblast differentiation into ECs and the pathway described in this report, which entails EC differentiation from the EMP lineage (Extended Data Fig. 10b). Multiple prior investigations have utilised *Csf1r-iCre* together with recombination reporters to follow the embryonic myeloid lineage 7, 10, 12. These studies predominantly employed FACS using hematopoietic markers, which precluded observation of *Csf1r-iCre*-targeted ECs. In contrast, we included EC markers in FACS protocols to additionally isolate *Csf1r-iCre*-targeted ECs. Additionally, immunostaining was previously used to identify *Csf1r-iCre*-targeted cells in the retina 17, liver and colon 18, but without description of EC targeting, possibly because of the close spatial proximity of ECs and perivascular macrophages 4, 33. We have overcome this limitation by performing high resolution imaging of tissues immunostained with both EC and MC markers. The contribution of EMP-derived ECs to yolk sac, brain, heart and lung vasculature is proportionally smaller than that of ECs of classical origin, whereas EMP-derived ECs predominate the liver, particularly the sinusoidal endothelium. Liver endothelium was previously reported to be heterogeneous in

origin, with an endoderm lineage contribution of approximately 15% and the remainder of the liver EC population attributed to a venous origin 34. Our results suggest that liver endothelium contains approximately 60% EMP-derived ECs. Preferential EMP homing to the liver after their entry into the embryonic circulation 13 and the dependence of liver growth on rapid vascular expansion 35 may explain the relatively large contribution of EMP-derived ECs to this organ. Ultimately, the discovery that EMPs provide a source of ECs for organ vasculature may open up new therapeutic avenues for vessel-dependent organ repair and regeneration. For example, EMPs or EMP-like EC progenitors, derived from human stem cells by modulating the expression of factors such as *Hoxa* genes, may be delivered systemically to support vascular growth in ischemic diseases or provide angiocrine signals that stimulate tissue stem cells.

Methods

Mouse strains

All animal procedures were performed in accordance with the institutional Animal Welfare Ethical Review Body (AWERB) and UK Home Office guidelines. To obtain mouse embryos of defined gestational age, mice were paired in the evening and the presence of a vaginal plug the following morning was defined as E0.5. In some studies, we analysed adult mice, defined as more than 8 weeks of age. Mice carrying the *Csf1r-iCre* transgene 18 were mated to the *Cre* recombination reporters $Rosa^{Yfp}$ 36, $Rosa^{tdTom}$ 37 or *CAG-cat-Egfp* 38 mice. $PU.1^{+/-}$ mice 39 were mated to $Rosa^{Yfp}$ mice and then *Csf1r-iCre* mice to obtain *Csf1r-iCre;*$Rosa^{Yfp}$*;*$Pu.1^{-/-}$ embryos that lack differentiated MCs including microglia 4, 39, 40 as well as the MC precursors of skin pericytes 41. $Hoxa^{fl/fl}$ mice 42 were mated to $Rosa^{tdTom}$ mice and then *Csf1r-iCre* to obtain *Csf1r-iCre;*$Rosa^{tdTom}$*;*$Hoxa^{fl/fl}$ embryos. *Csf1r-Mer-iCre-Mer* 19 and $Kit^{CreERT2}$ 43 as well as endothelial-specific *Cdh5-*$CreER^{T2}$ 41, 44 mice were mated to $Rosa^{tdTom}$ mice. In some experiments, mice carrying the *Csf1r-Egfp-Ngfr/Fkbp1a/Tnfrsf6* (short: *Csf1r-Egfp*) reporter of *Csf1r* expression 21 were mated to *Csf1r-Mer-iCre-Mer;*$Rosa^{tdTom}$ mice. We also used mice with a heterozygous loss of function mutation in *Csf1* (*Csf1*^{Op}) 45. All mouse strains were maintained on a mixed background (C57Bl6/J; 129/Sv), with the exception of *Csf1r-Mer-iCre-Mer*, which was maintained on a mixed FVB:C57/Bl6 background. For tamoxifen induction of CRE activity, tamoxifen (Sigma) was dissolved in peanut oil and administered via a single intraperitoneal injection into each pregnant dam. For *Csf1r-Mer-iCre-Mer* induction, we injected 1 mg tamoxifen; to achieve mosaic *Cdh5-Cre-*ER^{T2} activation, we injected 20 μg tamoxifen; for $Kit^{Cre\text{-}ERT2}$ induction at E8.5, we injected 3 mg tamoxifen together with 1.75 mg progesterone to increase induction without inducing abortions (Sigma).

Immunolabelling

Samples were fixed in 4% formaldehyde in PBS and processed as wholemounts or dehydrated in sucrose and embedded in optimal cutting temperature (OCT, Tissue-Tek) compound to cut 20 μm cryosections. Immunolabelling was performed as described previously for wholemount hindbrains 46. We used the following antibodies and dilutions: goat anti-CDH5 (1:200; AF1002, lot FQI0116101, R&D Systems), rabbit anti-CSF1R (1:500; sc-692, lot K1212, Santa Cruz), rat anti-EMCN (1:50; sc-65495, lot C2917, Santa

Cruz), rabbit anti-ERG (1:200; ab92513, lot GR32027 69-1, Abcam), rat anti-F4/80 (1:500; MCA497R, lot 1605, Serotec), chicken anti-GFP (1:1000; GFP-1020, lot 0511FP12, Aves) and rabbit anti-GFP (1:500; 598, lot 079, MBL) for YFP or EGFP labelling, rabbit anti-IBA1 (1:500; 019-19741, Wako Chemicals), rat anti-KIT (1:500; 553353, lot 30259, BD Pharmingen), rabbit anti-NG2 (1:200; AB5320, lot 2726769, Millipore), rat anti-PECAM1 (1:200; 553370, lot 5205656, BD Pharmingen), rabbit anti-pHH3 (1:400; 06-570, lot 2825969, Millipore), rabbit anti-RFP (1:1000; PM005, lot 045, MBL), goat anti-VEGFR2 (1:200; AF644, lot COA0417021, R&D Systems). Secondary antibodies used included Alexa Fluor-conjugated goat anti-chick, -rabbit or -rat IgG (Life Technologies), or, for primary antibodies raised in goat, donkey fluorophore-conjugated FAB fragments of anti-chick, -goat, -rabbit or -rat IgG (Jackson ImmunoResearch). Note that CDH5 47, ERG 48, EMCN 49, PECAM1 50 and VEGFR2 51 were used as EC markers, whereas F4/80 52 and IBA1 53 were used as macrophage markers and NG2 54 as a pericyte marker. Biotinylated IB4 (L2140, lot 085M4032V, Sigma) followed by Alexa-conjugated streptavidin (ThermoFisher) was also used to detect brain ECs and microglia 4, 16. Nuclei were labelled with DAPI. Images were acquired with a LSM710 laser scanning confocal microscope (Zeiss) and processed using LSM image browser (Zeiss) and Photoshop CS4 (Adobe) software. Three-dimensional rendering including surface rendering and the generation of virtual slices for lateral views of high-resolution confocal z-stacks was performed using Imaris (Bitplane). Z-stack projections of confocal images are shown unless indicated otherwise in the figure legends.

Fluorescence-activated cells sorting (FACS) and cell culture

Tissues were mechanically and enzymatically homogenised in RPMI1640 with 2.5% foetal bovine serum (ThermoFisher), 100 μg/ml collagenase/dispase (Roche), 50 μg/ml DNAse (Qiagen) and 100 μg/ml heparin (Sigma), incubated for 5 mins with 0.5 mg/ml rat Fc block (Becton Dickinson) and labelled with a combination of PE/Cy7-conjugated rat anti-PECAM1 (clone 390, cat 102418, lot B212262), FITC-conjugated rat anti-CD45 (clone 30-F11, cat 103108, lot B246762) or CD41 (clone MWReg30, cat 133903, lot B201955), APC-conjugated rat anti-KIT (clone 2B8, cat 105812, lot B217855) and PerCp/Cy5.5-conjugated rat anti-CD11b (clone M1/70, cat 101227) (all Biolegend). Appropriate fluorescence gating parameters were established with unstained tissue, *Csf1r-iCre*- or *Csf1r-Egfp*-negative tissues and fluorescence-minus-one (FMO) staining. For cell cycle analysis, cell populations were incubated with 10 μg/ml Hoechst 33342 (Sigma) for 30 mins at 37°C 55 before labelling with PE/Cy7-conjugated rat anti-PECAM1 and performing FACS analysis. In all experiments, doublets were eliminated using pulse geometry gates (FSC-H versus FSC-A and SSC-H versus SSC-A), whereas dead cells were removed using SYTOX Blue (Life Technologies) or LIVE/DEAD Fixable Violet (Life Technologies). Single cell suspensions were analysed using the BD LSRFortessa X-20 cell analyser or sorted using the BD Influx cell sorter (BD Biosciences); FlowJo software (FlowJo LLC) was used for subsequent analyses. In some experiments, a fraction of each population was cytospun onto a glass slide for Wright-Giemsa staining (Sigma) followed by imaging using an LSM510 microscope equipped with an AxioCam MRc camera (Zeiss). For cell culture experiments, cell populations were sorted into DMEM with 100 U/ml penicillin, 100 U/ml streptomycin and 20% foetal bovine serum (all ThermoFisher) before seeding the cells into a 96-well plate

coated with 10 μg/ml fibronectin (ThermoFisher) to facilitate EC differentiation. Cells were then cultured in methocult (Stemcell Technologies) to promote the formation of hematopoietic colonies, which were imaged using a TS100 microscope equipped with a DS-5M colour camera (Nikon). After removal of methocult, adherent cells were fixed with 4% formaldehyde in PBS and then labelled for VEGFR2, ERG, CD45, F4/80 and CSF1R (see above) before imaging using a Ti-E microscope (Nikon).

RNA-Seq

PECAM1^{+} CD45^{-} CD11b^{-} KIT^{-} ECs were isolated from E12.5 *Csf1r-Cre;Rosa*^{tdTom} embryos and divided into tdTom^{+} and tdTom^{-} populations with the BD Influx cell sorter before RNA was extracted with the RNeasy Micro Kit (QIAGEN). cDNA was generated and amplified using the SMART-seq V4 ultra low input RNA kit (Clontech). 100 pg of amplified cDNA per sample was used to prepare a library with the Nextera XT kit (Illumina) and run on the NextSeq 500 sequencer (lllumina). Raw sequence data were pre-processed to trim poor quality base calls and adapter contamination using Trimmomatic v.0.36.4 56 and aligned to the mouse mm10 genome with STAR v.2.5.2b 57. Mapped reads were deduplicated to reduce PCR bias using Picard v2.7.1.1 software (http://broadinstitute.github.io/picard/), and the reads-per-transcript were then calculated using FeatureCount v1.4.6.p5 software 58. Differential expression was performed using the BioConductor package DESeq2 via the SARTools wrapper v1.3.2.0 59.

Reverse transcription polymerase chain reaction (PCR)

We extracted RNA from cells isolated with the BD Influx cell sorter (see above) with the RNeasy Micro Kit for cDNA synthesis with Superscript IV (ThermoFisher). Quantitative (q) RT-PCR was performed with SYBR Green on an HT7900 system (Applied Biosystems) using the following oligonucleotide pairs: *Actb* 5'-CACCACACCTTCTACAATGAG-3' and 5'-GTCTCAAACATGATCTGGGTC-3'; *Cdh5* 5'-GATGCAGATGACCCCACTGT-3' and 5'-AGGGCATCTTGTGTTCCAC-3'; *Csf1r* 5'-TGCGTCTACACAGTTCAGAG-3' and 5'-ATGCTGTATATGTTCTTCGGT-3'; *Spi1* 5'-GCCATAGCGATCACTACTG-3' and 5'-CAAGGTTTGATAAGGGAAGC-3'; *Hoxa11* 5'-TCTTTGCCTCTCTCCTTCCTT-3' and 5'-TTGCAGACGCTTCTCTTTGTT-3'; *Evx1* 5'-GTGTGCTCTGGGCTCCTGT-3' and 5'-GCCAGGGTGCCTTGAGAG-3; *Slc2a1* 5'-CCCCAGAAGGTTATTGAGGAGT and 5'-ACAAAGAGGCCGACAGAGAA; *Mrc1* 5'-ACTGGGCAATGCAAATGGAG and 5'-CCCTCAAAGTGCAATGGACA; *Oit3* 5'-CGTCTGCTTCCATGTCTACTG and 5'-GTGCTCACATTCATTTTCGTCA. For each oligonucleotide pair, a no-template control reaction was included.

Microarray analysis

Published microarray data were used to compare gene expression levels (normalized log2OD) in E14.5 CD45^{-} PECAM1^{+} brain versus pooled lung and liver ECs (GSE35802) 22 and in HUVECs versus adult retinal ECs (GSE20986) 30 using GEO2R software (NCBI).

Europe PMC Funders Author Manuscripts

Statistical Analysis

Tissues for analysis were allocated to experimental groups according to genotype and gestational age. The number of YFP^+ ECs and YFP^+ microglia in *Csf1r-iCre;Rosa*^{Yfp} hindbrains (Fig. 1a,b and 1f-h) was determined in three randomly chosen 0.72 mm^2 regions of each wholemount labelled and flatmounted hindbrain. For hindbrains in *Hoxa*-targeting experiments, the number of $F4/80^+$ microglia (Extended Data Fig. 5) and $tdTom^+$ and $IB4^+$ volume (Fig. 5b,c) were determined from confocal z-stacks of four randomly chosen 0.18 mm^2 regions on the lateral side of each hindbrain (Extended Data Fig. 5g). The z-stacks were surface rendered with Imaris (Bitplane) to obtain the $F4/80^+$, $tdTom^+$ and $IB4^+$ volumes, and the $F4/80^+$ volume was then subtracted from both the $IB4^+$ and $tdTom^+$ total volume to obtain the $IB4^+$ EC and $tdTom^+$ EC volume before calculating the ratio of $tdTom^+$ to $IB4^+$ EC volume. To determine the number of vascular intersections in *Hoxa*-targeting experiments (Fig. 5b,d), the same confocal z-stacks were analysed with Imaris filament tracer after $F4/80^+$ microglia were masked. For Fig. 1 and Fig. 5, all counts obtained from one hindbrain were averaged to yield the value for that hindbrain; to ensure unbiased interpretation of results, the genotypes were disclosed only after data collection was complete. For all experiments, we calculated the mean value for at least 3 independent samples, where error bars represent the standard deviation of the mean (for details, see figure legends). Comparison of medians against means justified the use of a parametric test; to determine whether two datasets were significantly different, we therefore calculated p values with a two-tailed unpaired Student's t test; $P < 0.05$ was considered significant. When more than two data sets were compared, we used the statistical tests indicated in the associated figure legends. Statistical analyses were performed with Excel 12.2.6 (Microsoft Office) or Prism 5 (GraphPad Software).

Europe PMC Funders Author Manuscripts

Extended Data

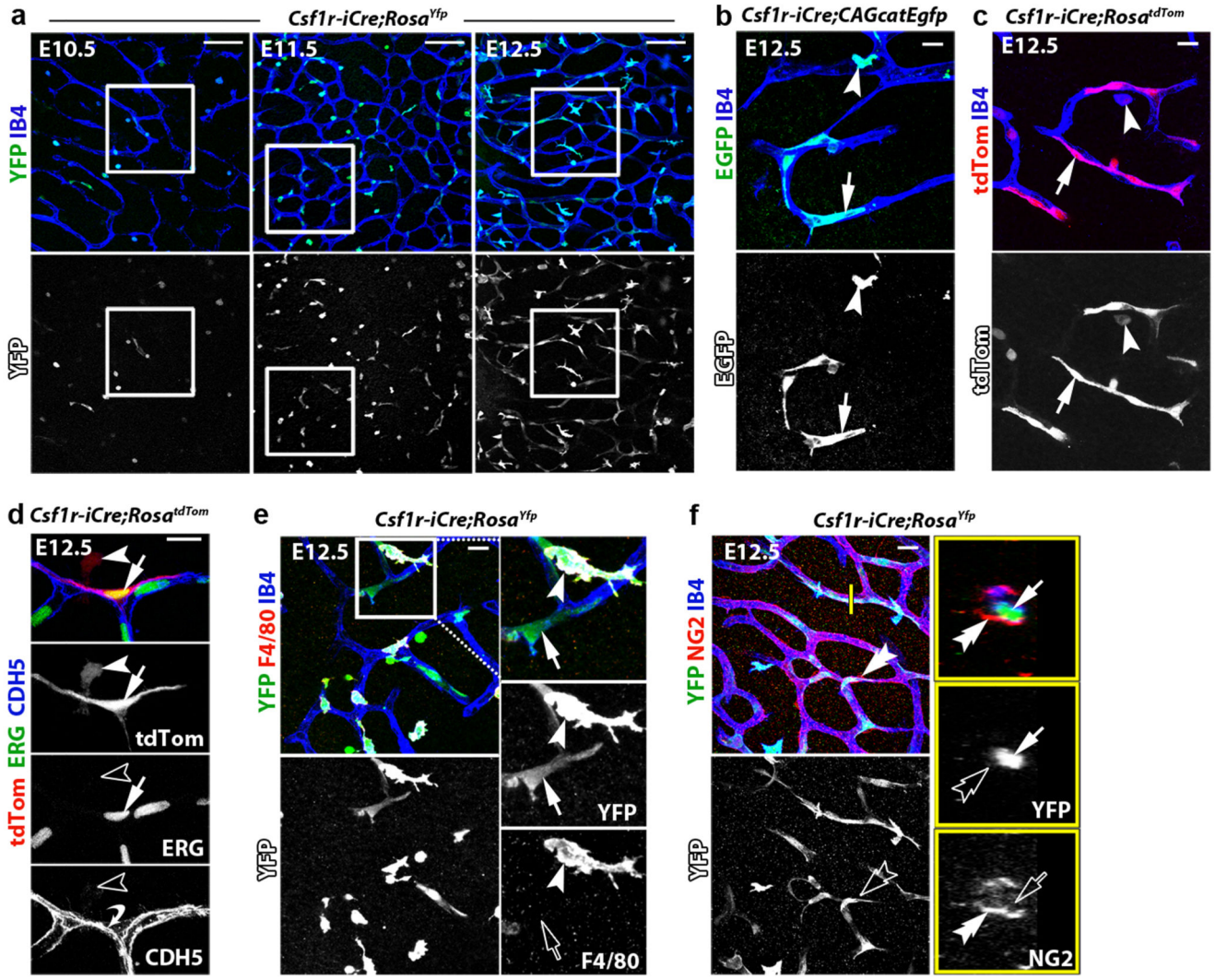

Extended data figure 1. Endothelial *Csf1r-iCre* targeting is observed with different recombination reporters and targeted ECs are distinguishable from macrophages and pericytes.

(**a-c**) *Csf1r-iCre;Rosa*^{Yfp} (**a**) *Csf1r-iCre;CAG-Cat-Egfp* (**b**) and *Csf1r-iCre;Rosa*^{tdTom} (**c**) hindbrains (n = 3 each) at the indicated stages were wholemount labelled with IB4 and for YFP (**a**) or GFP (**b**) or are shown together with tdTom fluorescence (**c**). In (**a**), the white squares indicate areas which were imaged at higher magnification for Fig. 1a. The indicated single channels are also shown individually.

(**d**) *Csf1r-iCre;Rosa*^{tdTom} E12.5 hindbrains (n = 3), wholemount labelled for ERG and CDH5 and shown including tdTom fluorescence to demonstrate that *Csf1r-iCre* targets ECs that form junctions with neighbouring ECs.

(**e,f**) E12.5 *Csf1r-iCre;Rosa*^{Yfp} hindbrains (n = 3), labelled for YFP and the microglia marker F4/80 (**e**) or the pericyte marker NG2 (**f**) together with IB4, show that *Csf1r-iCre-targeted* vessel-bound cells are neither microglia nor pericytes. In (**e**), the boxed area is shown in higher magnification and as single channels adjacent to the panel. In (**f**), a single

optical y/z cross section at the position indicated with the yellow line is displayed at higher magnification with single channels.

Symbols: Microglia and ECs are indicated with arrowheads and arrows, respectively, pericytes with double arrowheads, junctional CDH5 staining with a curved arrow; solid and clear symbols indicate the presence or absence of marker expression, respectively.

Scale bars: 100 μm (**a**), 20 μm (**b,c,e,f**), 50 μm (**d**).

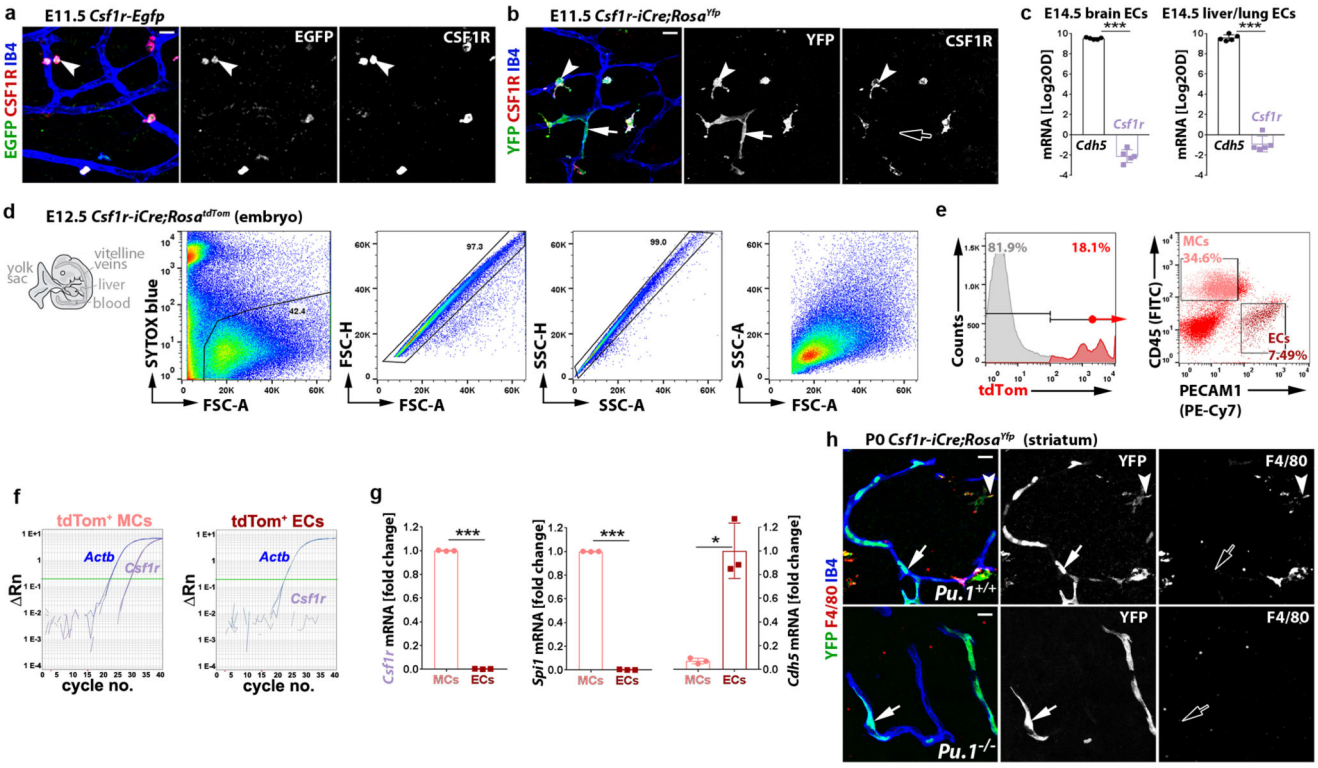

Extended data figure 2. Endothelial *Csf1r-iCre*-targeting is not caused by endothelial *Csf1r* expression and occurs independently of myeloid differentiation.

(**a,b**) *Csf1r-Egfp* (**a**) and *Csf1r-iCre;Rosa*^{Yfp} (**b**) E11.5 hindbrains (n = 3 each), wholemount labelled for CSF1R and EGFP or YFP together with IB4, show lack of *Csf1r* promoter activity and CSF1R protein in ECs.

(**c**) Graphic representation of relative *Cdh5* and *Csf1r* expression levels in E14.5 brain or pooled lung/liver EC microarrays 22; n = 5 each; ***P < 0.0001 (two-tailed unpaired t-test).

(**d-g**) FACS separation of tdTom$^+$ cells from *Csf1r-iCre;Rosa*^{tdTom} embryos (n = 3) for gene expression analysis, including (**d**) representative gating strategy to exclude dead cells and doublets in this and subsequent experiments and (**e**) sorting into PECAM1$^+$ CD45$^-$ ECs versus CD45$^+$ PECAM1$^-$ MCs. (**f**) Representative RT-qPCR gene amplification graphs for *Csf1r* versus *Actb* from tdTom$^+$ MCs and ECs; ΔRn, normalised reporter value for SYBR Green minus baseline instrument signals. (**g**) Graphic representation of the fold change in RT-qPCR amplification of the indicated genes relative to *Actb* for both cell populations; each data point represents one embryo; *P = 0.0242, ***P < 0.0001 (two-tailed unpaired t-test).

Europe PMC Funders Author Manuscripts

(**h**) *Csf1r-iCre;Rosa*^{Yfp} P0 striatum on a *Pu.1*$^{+/+}$ versus *Pu.1*$^{-/-}$ background (n = 3 brains each), cryo-sectioned and labelled for YFP and F4/80 together with IB4 to show that *Csf1r-iCre*-targeted ECs are PU.1-independent and persist postnatally.

Symbols: Arrowheads indicate microglia, arrows YFP^{+} ECs, clear arrows YFP^{+} ECs that are CSF1R^{-} and F4/80^{-}.

Scale bars: 20 μm.

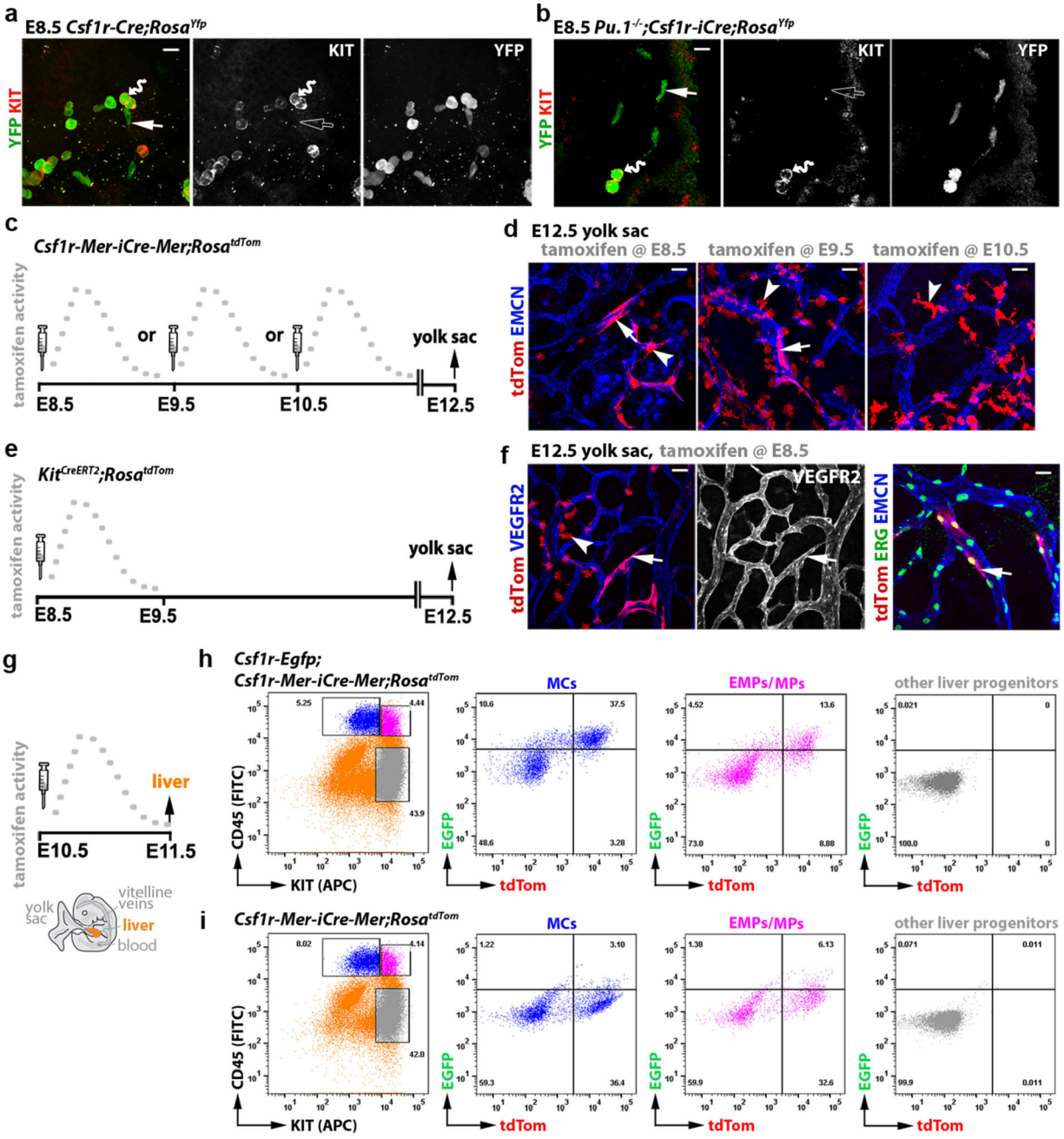

Extended data figure 3. Lineage tracing of yolk sac and liver EMPs.

Europe PMC Funders Author Manuscripts

(**a,b**) E8.5 wild type (**a**) and *Pu.1*$^{-/-}$ (**b**) yolk sacs on a *Csf1r-iCre;Rosa*^{Yfp} background (n = 3 yolk sacs each), wholemount labelled for YFP and KIT, show *Csf1r-iCre*-targeted KIT^{+} round cells corresponding to EMPs/MPs and *Csf1r-iCre*-targeted KIT^{-} flat cells corresponding to ECs. *Scale bars*: 20 μm.

(**c-f**) Pregnant *Csf1r-Mer-iCre-Mer;Rosa*^{tdTom} (**c,d**) and *Kit*$^{CreERT2;}$*Rosa*^{tdTom} (**e,f**) dams were injected with a single tamoxifen dose on the indicated days; E12.5 yolk sacs were wholemount labelled for the indicated markers to identify *Csf1r-iCre*-targeted ECs and macrophages (n = 3 yolk sacs for each genotype). *Symbols*: Wavy arrows indicate EMPs, straight arrows *Csf1r-iCre*-lineage-traced ECs, arrowheads macrophages. Solid and clear symbols indicate the presence or absence, respectively, of the indicated markers. *Scale bars*: 20 μm.

(**g-i**) Pregnant dams were injected with a single tamoxifen dose on E10.5 (**g**) before FACS analysis of E11.5 *Csf1r-Egfp;Csf1r-Mer-iCre-Mer;Rosa*^{tdTom} (**h**) or *Csf1r-Mer-iCre-Mer;Rosa*^{tdTom} control (**i**) livers (n = 4 each) for the indicated markers; the CD45^{hi} KIT^{-} differentiated MCs (blue), CD45^{lo} KIT^{+} EMP/MP population (pink) and the CD45^{-} KIT^{+} population (grey) were gated further for *Csf1r-Egfp* and tdTom. CD45^{-} KIT^{+} cells were neither MCs nor EMPs, because they lacked CD45, tdTom and EGFP.

Europe PMC Funders Author Manuscripts

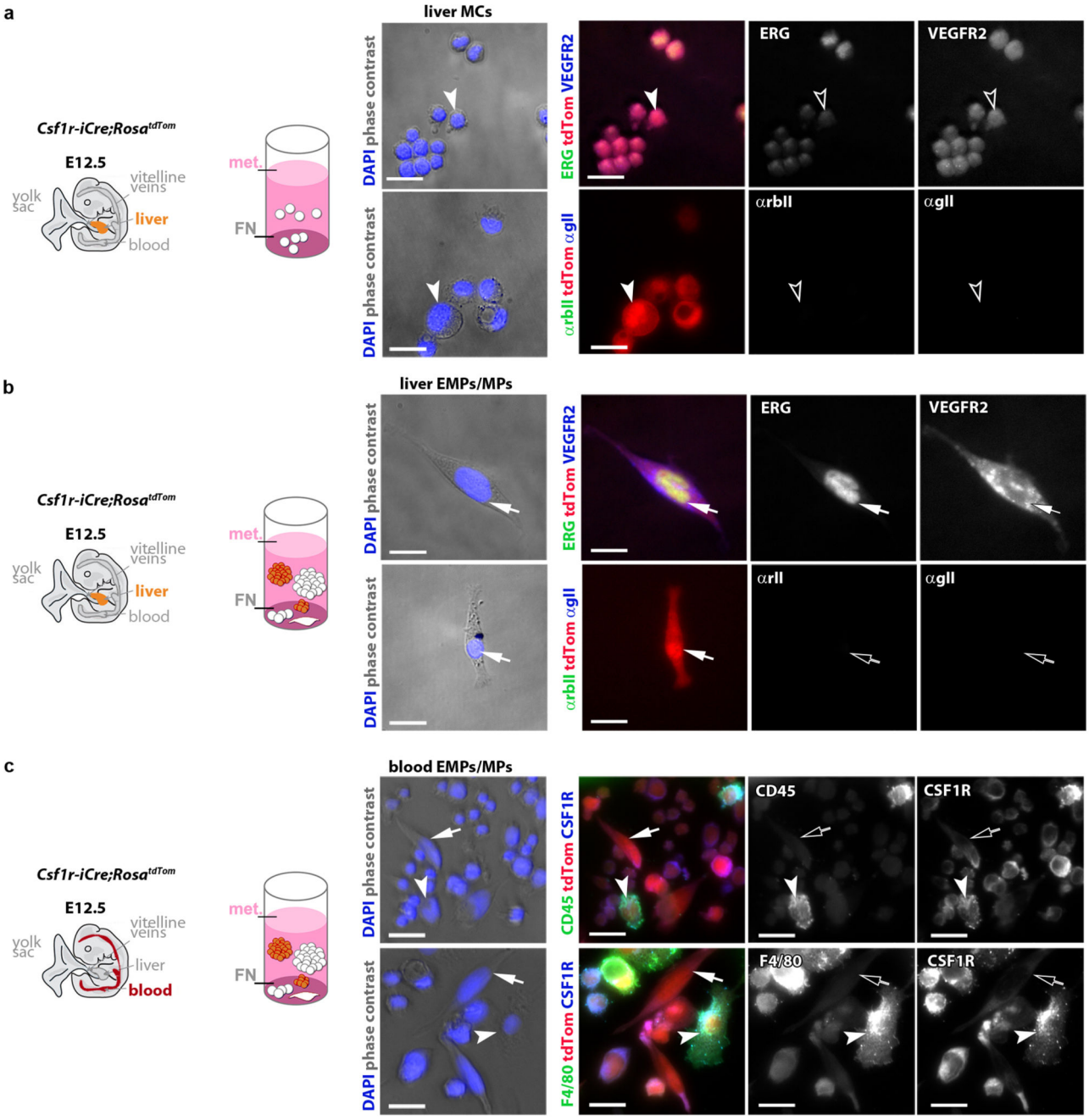

Extended data figure 4. Immunostaining controls for cultured *Csf1r-iCre*-targeted cells.

The indicated cell populations were FACS-isolated from E12.5 *Csf1r-iCre;Rosa*^{tdTom} liver or blood with the indicated markers and cultured for three days in methocult (met.) on fibronectin (FN); n = 1 experiment. Adherent cells from tdTom^{+} liver MC (**a**) and EMP/MP (**b**) cultures were stained for ERG and VEGFR2 (top panels) or with secondary antibodies only (bottom panels). In (**c**), adherent cells from tdTom^{+} blood EMP/MP cultures were immunostained for CSF1R together with the myeloid markers CD45 (top panels) or F4/80 (bottom panels). In the first panel in each row, the phase contrast and DAPI images were

Europe PMC Funders Author Manuscripts

merged. In panels 2-4 in each row, immunolabelled cells were visualised together with tdTom fluorescence, with single channels for the indicated markers shown separately in grey scale. *Symbols*: Arrows indicate tdTom$^+$ ECs, arrowheads tdTom$^+$ myeloid cells; solid and clear symbols indicate the presence or absence, respectively, of the indicated markers. *Scale bars*: 20 μm.

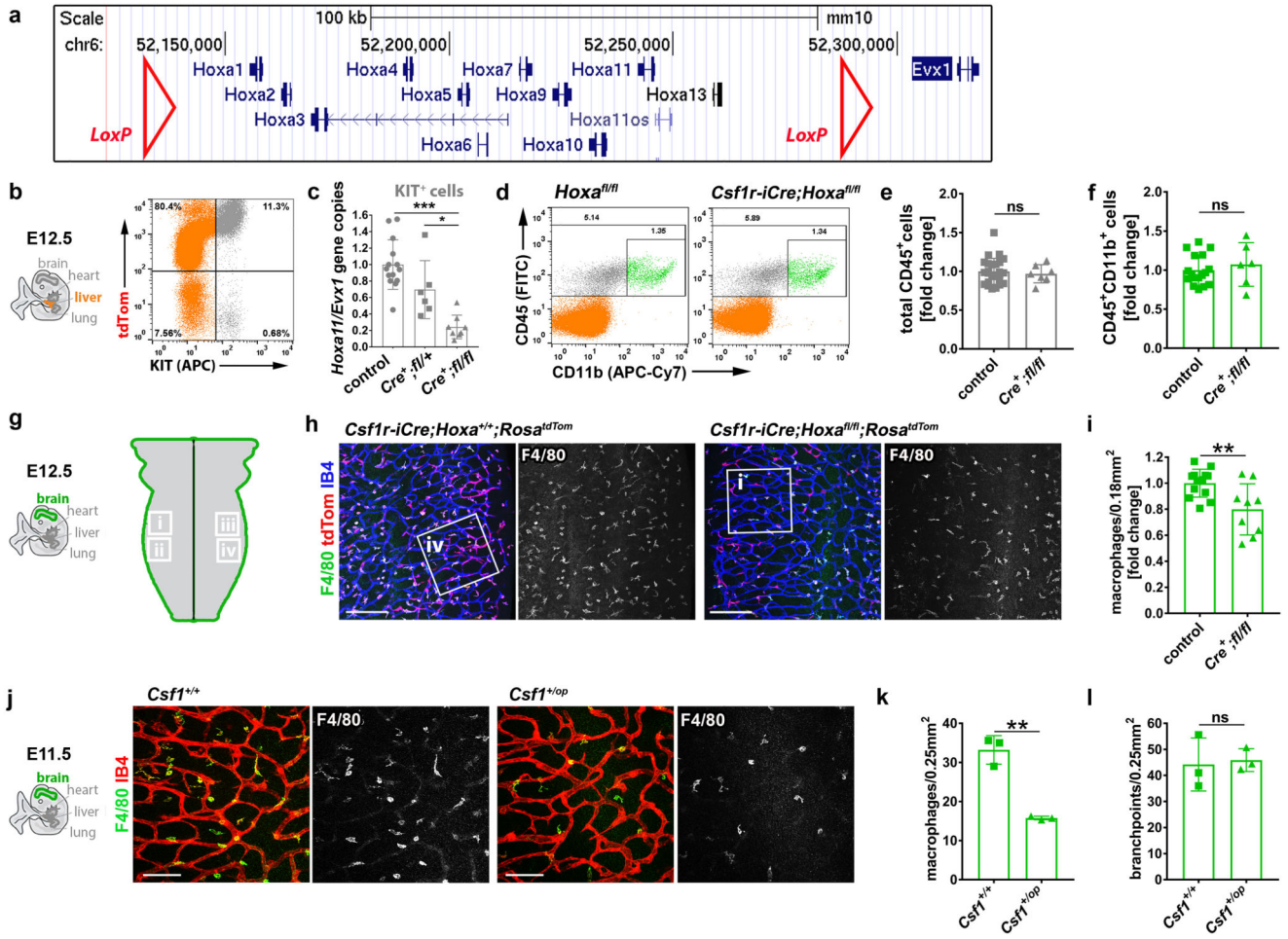

Extended data figure 5. *Hoxa* gene targeting with *Csf1r-iCre*.

(**a**) Schematic representation of the *Hoxa* gene cluster and adjacent *Evx1* gene using the UCSC Genome Browser with the mouse December 2011 (GRCm38/mm10) Assembly, including position of the *LoxP* sites used for gene targeting.

(**b-c**) Validation of *Hoxa* targeting. (**b**) FACS strategy to isolate KIT$^+$ cells from E12.5 control (pooled *Csf1r-iCre*$^-$ or *Csf1r-iCre*$^+$;*Hoxa*$^{+/+}$; n = 14), *Hoxa*$^{+/fl}$;*Csf1r-iCre* (n = 6) and *Hoxa*$^{fl/fl}$;*Csf1r-iCre* (n = 8) livers. (**c**) qPCR analysis of *Hoxa* gene copy number relative to *Evx1*; data are shown as mean ± SD; each symbol represents the value for one individual liver; * P=0.0156, *** P<0.001 (1-way ANOVA, Tukey's multiple comparisons test).

(**d-f**) Representative FACS analysis (**d**) and quantification (**e,f**) of liver cell populations at E12.5 shows a similar number of total CD45$^+$ and CD45$^+$ CD11b$^+$ differentiated MCs in *Hoxa*$^{fl/fl}$;*Csf1r-iCre* mutants (n = 7 for CD45$^+$; n = 6 for CD45$^+$ CD11b$^+$) versus pooled

Europe PMC Funders Author Manuscripts

Europe PMC Funders Author Manuscripts

Csf1r-iCre^{-} and *Csf1r-iCre*$^{+}$;*Hoxa*$^{+/+}$controls (n = 25 for CD45^{+}, n = 17 for CD45^{+} CD11b^{+}); data are shown as mean ± SD fold change in mutants compared to controls; each data point represents one liver; ns, non-significant, P = 0.6519 (**e**) and P = 0.496 (**f**), (two-tailed unpaired t-test).

(**g-i**) E12.5 hindbrains of the indicated genotypes were immunolabelled to determine vascular complexity and quantify microglia. (**g**) Schematic representation of a wholemount embryonic hindbrain (left) and location of the hindbrain areas i-iv used for quantification in each hindbrain (right); values for the four areas in each hindbrain were averaged to obtain the value for that hindbrain; EC quantifications are shown in Fig. 5c. (**h**) Hindbrains were wholemount labelled with IB4 and for RFP to visualise tdTom and for F4/80 to visualise microglia; white boxes indicate areas shown in higher magnification in Fig. 5. (**i**) Quantification of microglia number in *Hoxa*$^{fl/fl}$;*Csf1r-iCre* mutants (n = 9) versus controls (n = 10, pooled *Csf1r-iCre*$^{+}$;*Hoxa*$^{+/+}$ and *Csf1r-iCre*$^{-}$ of any *Hoxa* genotype); mean ± SD fold change in mutant compared to control hindbrain; each data point represents one hindbrain; **P = 0.0055 (two-tailed unpaired t-test).

(**j-l**) E11.5 *Csf1*$^{+/+}$ and *Csf1*$^{+/op}$ littermate hindbrains, wholemount labelled for F4/80 together with IB4 (**j**) before quantification of microglia (**k**) and vascular branchpoint (**l**) number as a measure of vascular complexity. Mean ± SD; each data point represents the value for one hindbrain, n=3 each; ns, non-significant, P = 0.808, **P = 0.0012 (two-tailed unpaired t-test).

Scale bars: 200 μm (**h**), 100 μm (**j**).

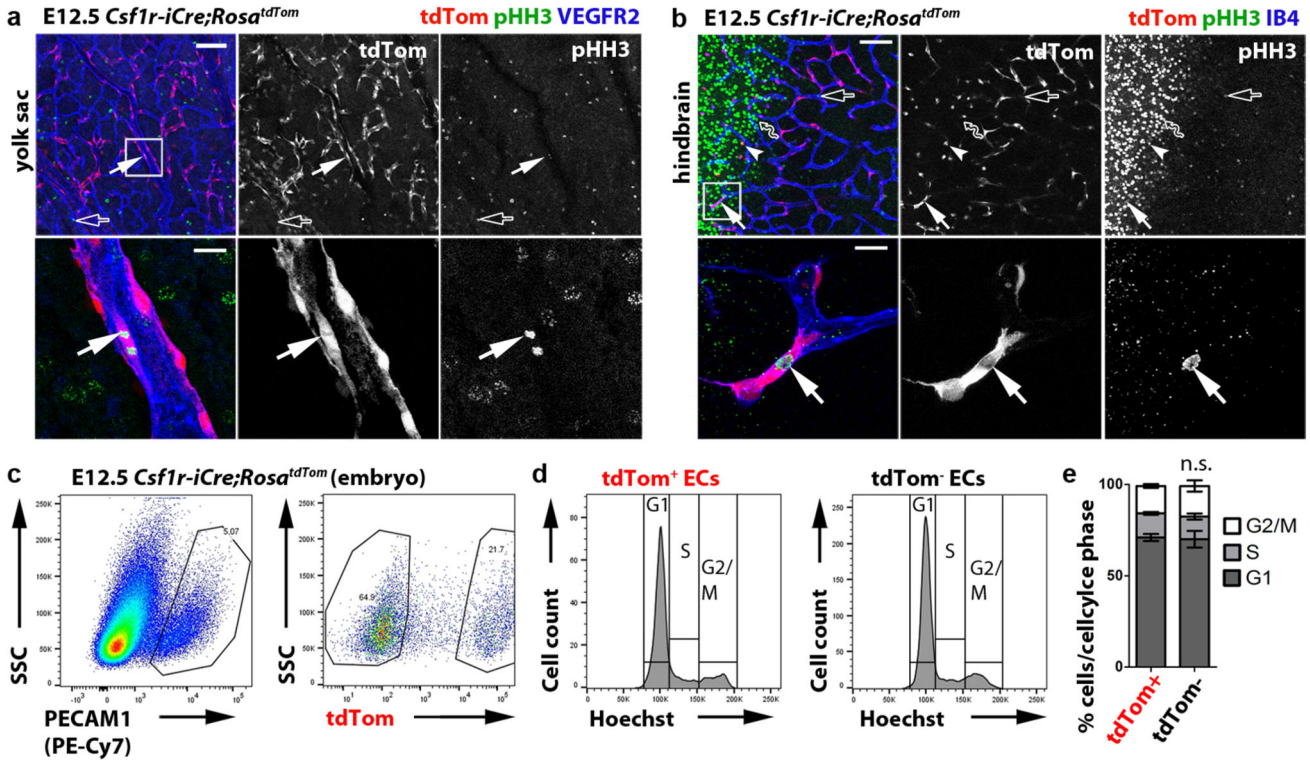

Extended data figure 6. *Csf1r-iCre*-targeted ECs proliferate in vivo.

(**a,b**) E12.5 *Csf1r-iCre;Rosa*^{tdTom} yolk sac (**a**) or hindbrain (**b**), wholemount stained for the proliferation marker pHH3 and VEGFR2 or for pHH3 together with IB4, respectively, and shown together with tdTom fluorescence (n = 3 each). Areas indicated with white squares were imaged at higher magnification and are shown below the corresponding panel, with tdTom and pHH3 channels also shown separately in grey scale. *Symbols*: The arrows indicate proliferating tdTom^{+} pHH3^{+} ECs; solid and clear symbols indicate the presence or absence, respectively, of tdTom fluorescence; the wavy arrow indicates a tdTom^{-} pHH3^{+} neural progenitor. *Scale bars*: 100 μm (top panels), 20 μm (lower panels).
(**c-e**) *Cell cycle distribution of tdTom*$^{+}$ *and tdTom*$^{-}$ *ECs*. (**c**) FACS strategy to isolate tdTom^{+} and tdTom^{-} PECAM1^{+} ECs from E12.5 *Csf1r-iCre;Rosa*^{tdTom} embryos (n = 3 embryos). (**d**) Graphic representation of cell cycle distribution based on Hoechst 33342 fluorescence as a measure of DNA content; low and high staining intensity is observed in cells with a DNA ploidy of 2n (G0/G1 phase) or 4n (G2/M phase), respectively; an intermediate staining intensity corresponds to S phase. (**e**) Mean ± SD proportion of tdTom^{+} and tdTom^{-} ECs in G1, S and G2/M based on the area of the corresponding peaks in (**d**); n.s., non-significant, P > 0.9999 (two-way ANOVA, Bonferroni's multiple comparisons test).

Europe PMC Funders Author Manuscripts

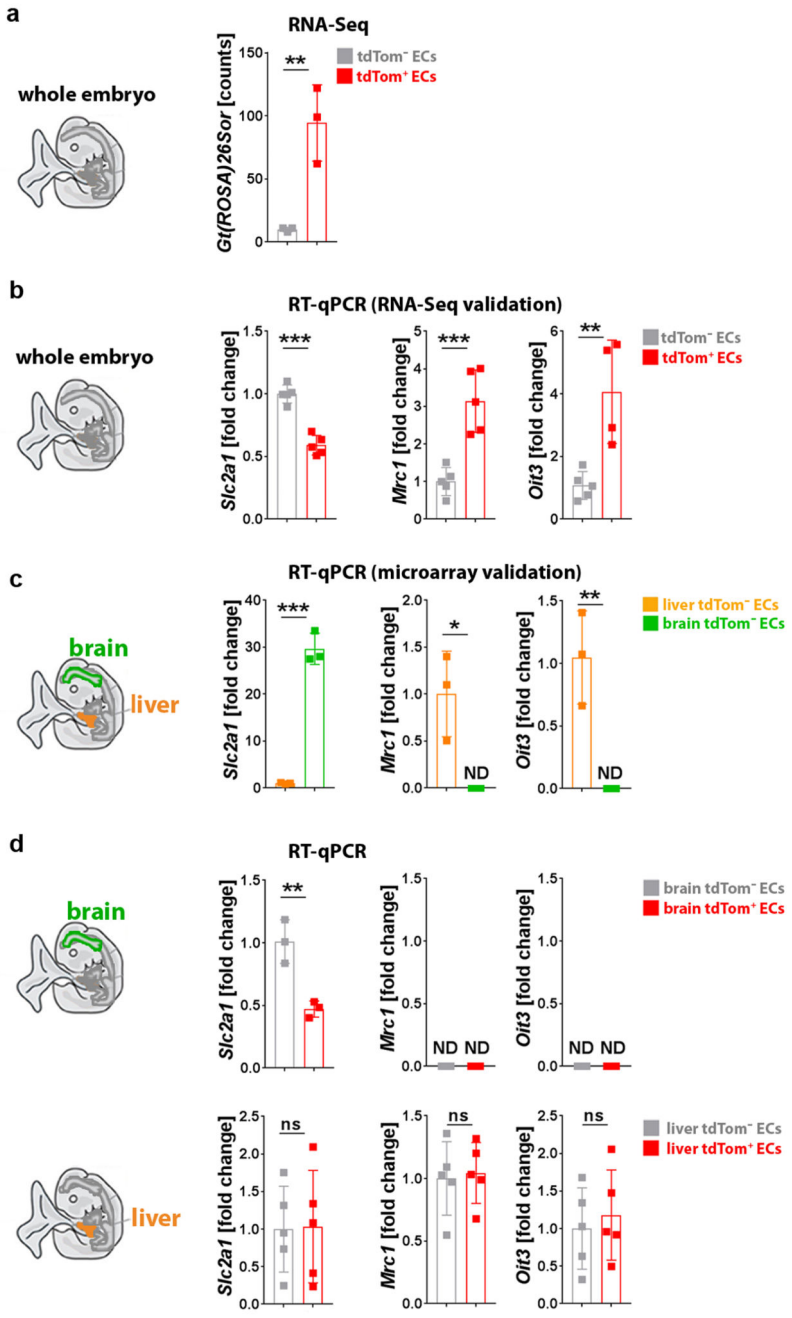

Extended data figure 7. Validation of gene expression data from RNA-Seq and microarray studies.

ECs were FACS-isolated from E12.5 *Csf1r-iCre;Rosa*^{tdTom} embryos (n = 3) as in Fig. 6a to validate the RNA-Seq and microarray data shown in Fig. 6d-f. *Slc2a1* was analysed as a representative brain EC-enriched transcript/differentiation marker, *Mrc1* and *Oit3* as representative liver EC-enriched transcripts.

(**a**) Relative transcript levels of the *Gt(ROSA)26Sor* (*tdTomato*) transcript by RNA-Seq of the E12.5 tdTom^{+} and tdTom^{-} EC populations, whose analysis is presented in Fig. 6a-f; mean ± SD of normalised counts, n = 3 each; **P = 0.0085 (two-sided unpaired t-test).

Europe PMC Funders Author Manuscripts

(**b**) RT-qPCR analysis for the indicated genes in tdTom$^+$ versus tdTom$^-$ ECs isolated from whole E12.5 embryos (n = 5) to validate genes identified by RNA-Seq in Fig. 6e,f as differentially expressed. Mean ± SD of fold change; ***P < 0.0001 (*Slc2a1*), ***P = 0.0008 (*Mrc1*) **P = 0.0056 (*Oit3*) (two-sided unpaired t-test).

(**c**) RT-qPCR analysis for the indicated genes in tdTom$^-$ ECs isolated from the E12.5 brain versus liver (n = 3 for each organ) to validate organ-specific transcript enrichment identified via microarray analysis shown in Fig. 6f. Mean ± SD of fold change; *P = 0.019, **P = 0.0082, ***P < 0.0001 (two-sided unpaired t-test); ND, not detectable.

(**d**) RT-qPCR analysis for the indicated genes to directly compare the expression levels of brain and liver EC differentiation markers in tdTom$^+$ versus tdTom$^-$ ECs isolated from brain (n = 3) or liver (n=5). Mean ± SD of fold change; ns, non-significant, P = 0.9398 (liver *Slc2a1*), P = 0.8045 (liver *Mrc1*), P = 0.6327 (liver *Oit3*), **P = 0.0073 (brain *Slc2a1*) (two-sided unpaired t-test); ND, not detectable.

Europe PMC Funders Author Manuscripts

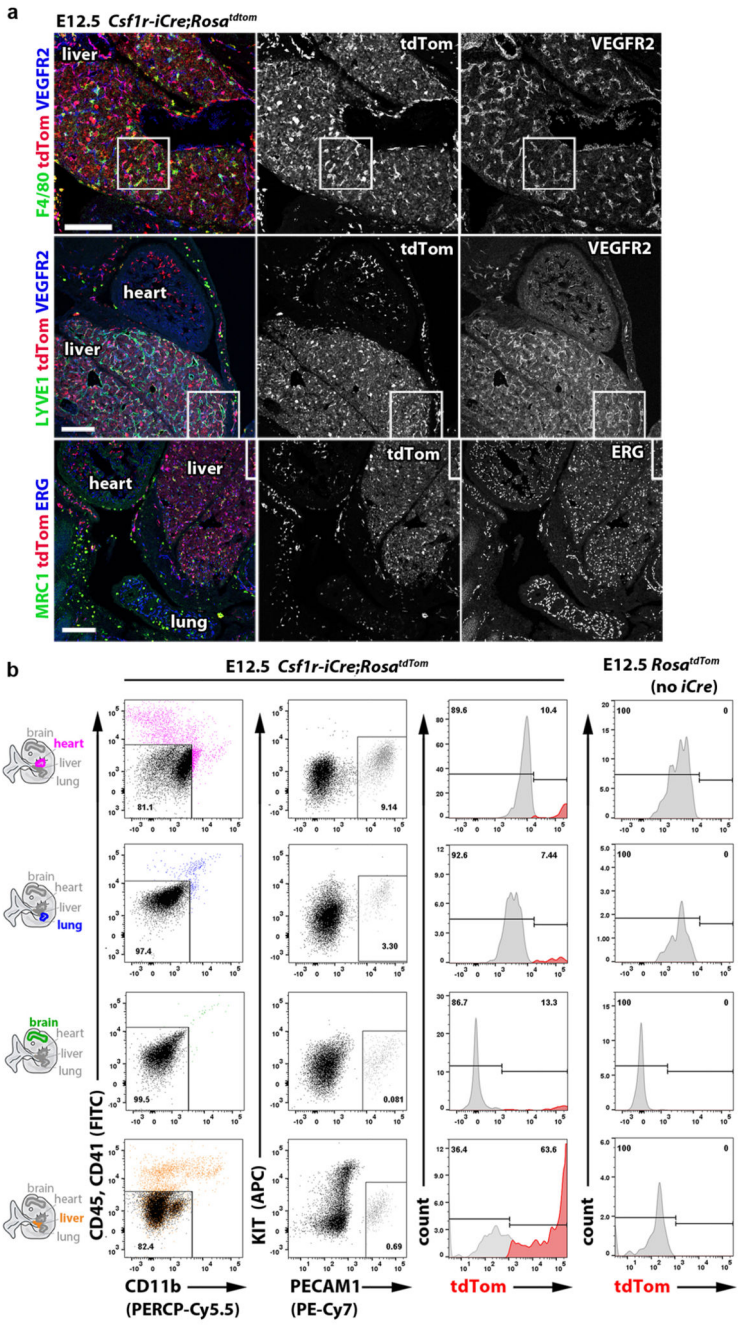

Extended data figure 8. *Csf1r-iCre*-targeted ECs contribute to embryonic vasculature in multiple organs.

(**a**) 20 μm cryosections of the indicated E12.5 *Csf1r-iCre;Rosa*^{tdTom} organs (n = 3 each) were immunolabelled for the indicated EC markers together with antibodies for RFP to identify tdTom protein (top and bottom panels) or are shown with tdTom fluorescence (middle panels); single channels are shown in grey scale. The white boxes indicate the position of areas shown in higher magnification in Fig. 6g; note that some areas selected for

higher magnification are not contained entirely within the field of view, and accordingly the boxes are shown incomplete. *Scale bars:* 200 μm.

(**b**) Gating strategy for FACS analysis of tdTom^{+} and tdTom^{-} ECs from E12.5 *Csf1r-iCre;Rosa*^{tdTom} brain, lung, heart and liver and control organs lacking *iCre*, using antibodies for CD11b, CD41, CD45, KIT, PECAM1; associated EC quantifications are shown in Fig. 6i. An analogous strategy was used for the quantifications shown in Fig. 6j and in the Extended Data Fig. 9b.

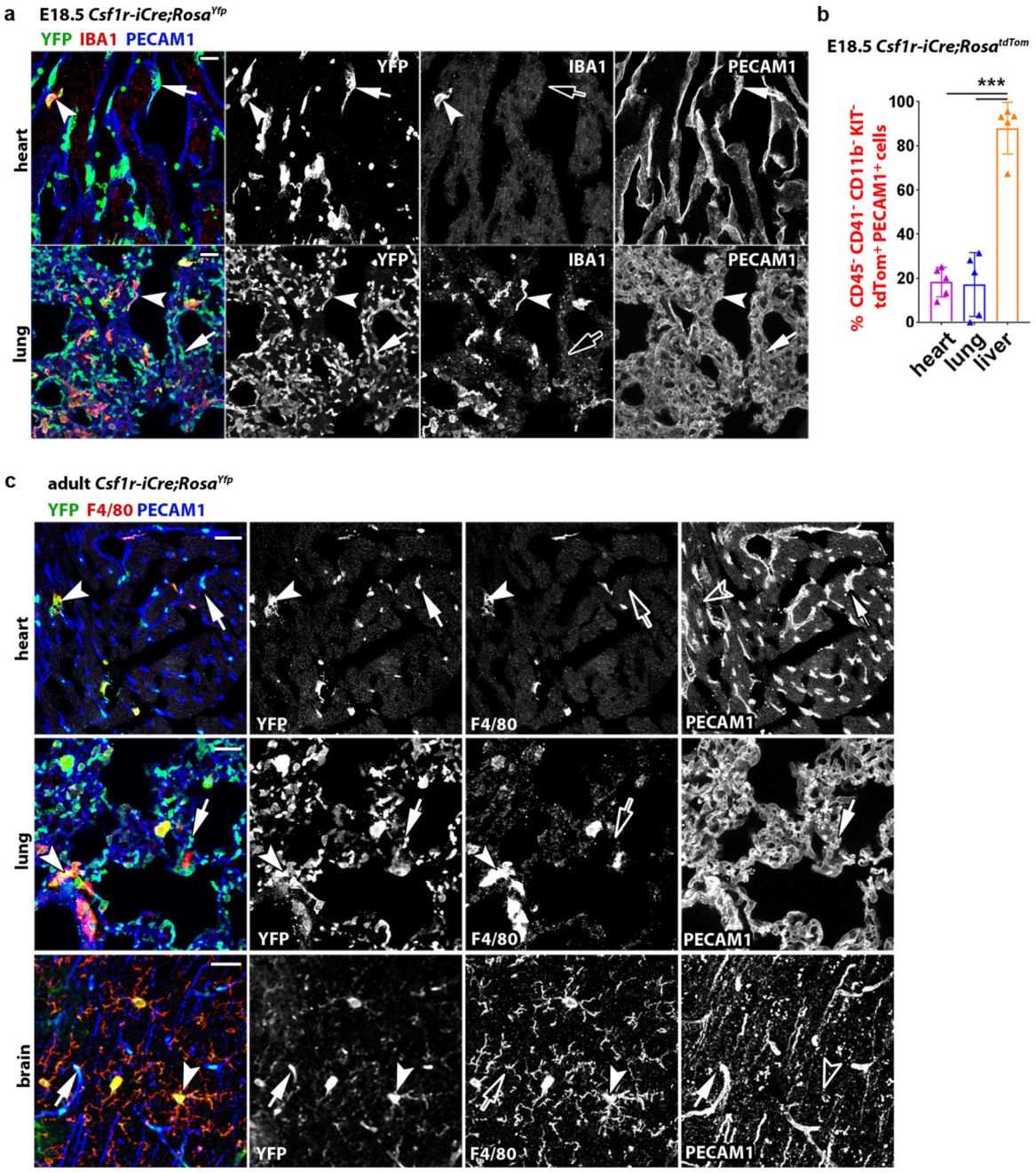

Europe PMC Funders Author Manuscripts

Europe PMC Funders Author Manuscripts

Extended data figure 9. *Csf1r-iCre*-targeted ECs contribute to organ vasculature in late stage embryos and adults.

(**a**) 20 μm cryosections of the indicated organs from E18.5 *Csf1r-iCre;Rosa*^{Yfp} mice (n = 2 each) were immunolabelled for YFP, the EC marker PECAM1 and the macrophage marker IBA1; single channels are shown in grey scale. *Symbols*: Arrowheads indicate YFP^{+} IBA1^{+} macrophages; solid and empty arrows indicate ECs that are YFP^{+} and lack IBA1 expression, respectively. *Scale bars*: 20 μm.

(**b**) Flow cytometry of dissociated cells from the indicated organs of E18.5 *Csf1r-iCre;Rosa*^{tdTom} embryos after staining with antibodies for CD11b, CD41, CD45, KIT, PECAM1, using the gating strategy shown in the Extended data Fig. 8b; mean ± SD, n = 5 each; ***P < 0.0001 (1-way ANOVA, Tukey's multiple comparisons test).

(**c**) 20 μm cryosections of the indicated organs from 6 months old adult *Csf1r-iCre;Rosa*^{Yfp} mice (n = 3 organs each) were immunolabelled for YFP, the EC marker PECAM1 and the macrophage marker F4/80; single channels are shown in grey scale. *Symbols*: Arrowheads indicate YFP^{+} and F4/80^{+} macrophages; solid and empty arrows indicate ECs that are YFP^{+} and lack F4/80 expression, respectively. *Scale bars*: 20 μm.

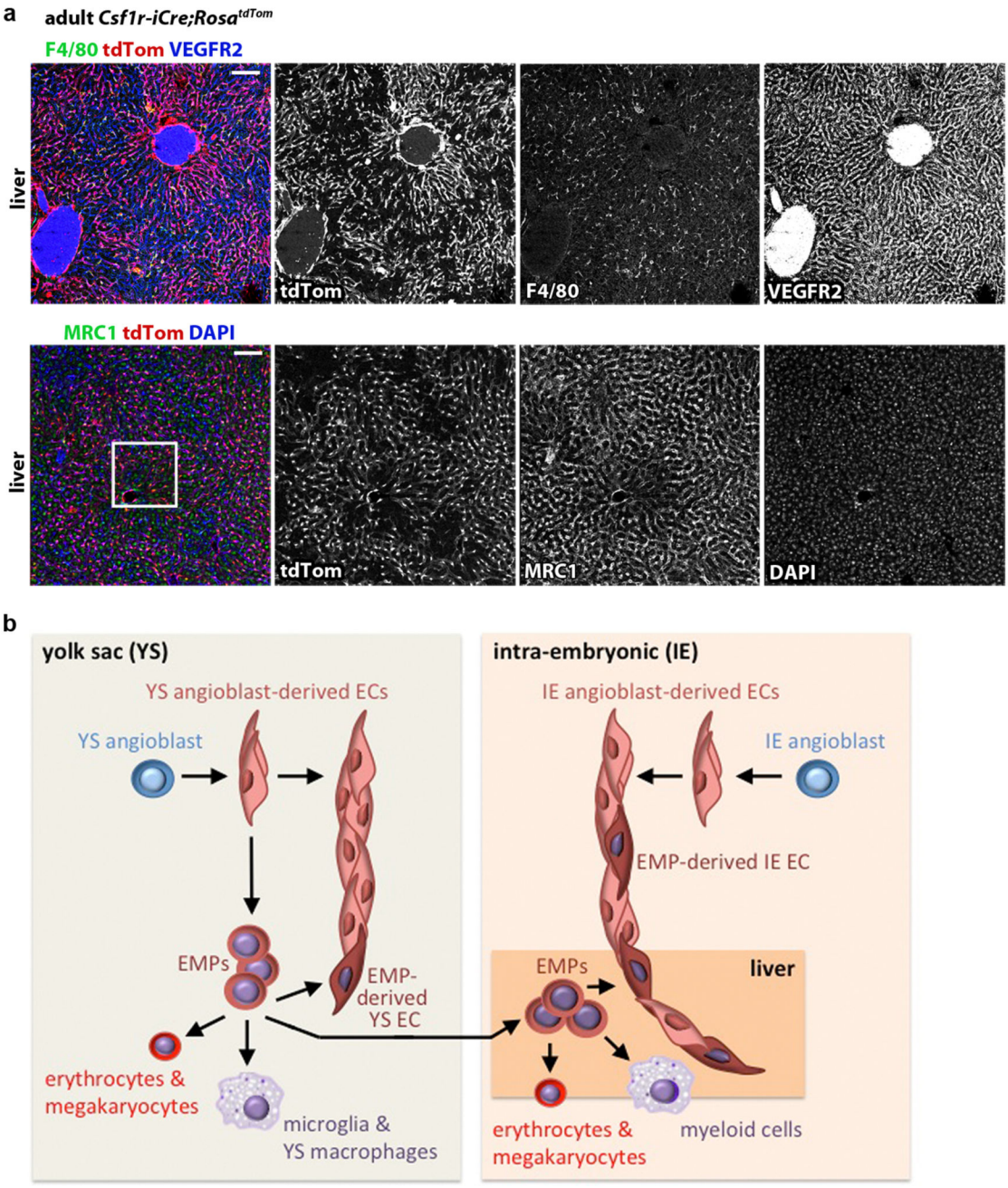

Extended data figure 10. *Csf1r-iCre*-targeted ECs contribute to adult organ vasculature.

(**a**) 20 μm cryosections of 3 months old adult *Csf1r-iCre;Rosa*^{tdTom} livers (n = 3) were immunolabelled for RFP and the EC marker VEGFR2 and the macrophage marker F4/80 or the liver EC sinusoidal EC marker MRC1 and then counterstained with DAPI; single channels are shown in grey scale. The white box indicates an area shown in higher magnification in Fig. 6h. *Scale bars*: 100 μm.

(**b**) Working model for the role of EMPs in generating extra-embryonic yolk sac and intra-embryonic organ ECs alongside their known role in generating myeloid and erythrocyte/megakaryocyte cells.

Supplementary Material

Refer to Web version on PubMed Central for supplementary material.

Acknowledgements

We thank the Biological Resources, FACS, Imaging and Genomics facilities at UCL and E. Scarpa for technical help, D. Saur, A. Mass, D. Duboule, M. Kmita and Y. Kubota for mouse strains and M. Golding for helpful discussions. This research was supported by grants from the Wellcome Trust (095623/Z/11/Z, 101067/Z/13/Z), Medical Research Council (MR/N011511/1) and British Heart Foundation (FS/17/23/32718).

References

1. Potente M, Gerhardt H, Carmeliet P. Basic and therapeutic aspects of angiogenesis. Cell. 2011; 146:873–887. [PubMed: 21925313]
2. Hirschi KK, Ingram DA, Yoder MC. Assessing identity, phenotype, and fate of endothelial progenitor cells. Arteriosclerosis, Thrombosis, and Vascular biology. 2008; 28:1584–1595.
3. Pollard JW. Trophic macrophages in development and disease. Nature Reviews. Immunology. 2009; 9:259–270.
4. Fantin A, et al. Tissue macrophages act as cellular chaperones for vascular anastomosis downstream of VEGF-mediated endothelial tip cell induction. Blood. 2010; 116:829–840. [PubMed: 20404134]
5. Clausen BE, Burkhardt C, Reith W, Renkawitz R, Forster I. Conditional gene targeting in macrophages and granulocytes using LysMcre mice. Transgenic Research. 1999; 8:265–277. [PubMed: 10621974]
6. de Boer J, et al. Transgenic mice with hematopoietic and lymphoid specific expression of Cre. European Journal of Immunology. 2003; 33:314–325. [PubMed: 12548562]
7. Hoeffel G, et al. C-Myb(+) erythro-myeloid progenitor-derived fetal monocytes give rise to adult tissue-resident macrophages. Immunity. 2015; 42:665–678. [PubMed: 25902481]
8. Frame JM, McGrath KE, Palis J. Erythro-myeloid progenitors: "definitive" hematopoiesis in the conceptus prior to the emergence of hematopoietic stem cells. Blood Cells, Molecules & Diseases. 2013; 51:220–225.
9. Mass E, et al. Specification of tissue-resident macrophages during organogenesis. Science. 2016; 353
10. Gomez Perdiguero E, et al. Tissue-resident macrophages originate from yolk-sac-derived erythro-myeloid progenitors. Nature. 2015; 518:547–551. [PubMed: 25470051]
11. McGrath KE, et al. Distinct Sources of Hematopoietic Progenitors Emerge before HSCs and Provide Functional Blood Cells in the Mammalian Embryo. Cell reports. 2015; 11:1892–1904. [PubMed: 26095363]
12. Schulz C, et al. A lineage of myeloid cells independent of Myb and hematopoietic stem cells. Science. 2012; 336:86–90. [PubMed: 22442384]
13. Ginhoux F, Guilliams M. Tissue-Resident Macrophage Ontogeny and Homeostasis. Immunity. 2016; 44:439–449. [PubMed: 26982352]
14. Hoeffel G, Ginhoux F. Fetal monocytes and the origins of tissue-resident macrophages. Cell Immunol. 2018
15. Lux CT, et al. All primitive and definitive hematopoietic progenitor cells emerging before E10 in the mouse embryo are products of the yolk sac. Blood. 2008; 111:3435–3438. [PubMed: 17932251]
16. Fantin A, et al. NRP1 acts cell autonomously in endothelium to promote tip cell function during sprouting angiogenesis. Blood. 2013; 121:2352–2362. [PubMed: 23315162]

17. Stefater JA 3rd, et al. Regulation of angiogenesis by a non-canonical Wnt-Flt1 pathway in myeloid cells. Nature. 2011; 474:511–515. [PubMed: 21623369]
18. Deng L, et al. A novel mouse model of inflammatory bowel disease links mammalian target of rapamycin-dependent hyperproliferation of colonic epithelium to inflammation-associated tumorigenesis. The American Journal of Pathology. 2010; 176:952–967. [PubMed: 20042677]
19. Qian BZ, et al. CCL2 recruits inflammatory monocytes to facilitate breast-tumour metastasis. Nature. 2011; 475:222–225. [PubMed: 21654748]
20. Sasmono RT, et al. A macrophage colony-stimulating factor receptor-green fluorescent protein transgene is expressed throughout the mononuclear phagocyte system of the mouse. Blood. 2003; 101:1155–1163. [PubMed: 12393599]
21. Burnett SH, et al. Conditional macrophage ablation in transgenic mice expressing a Fas-based suicide gene. Journal of Leukocyte Biology. 2004; 75:612–623. [PubMed: 14726498]
22. Tam SJ, et al. Death receptors DR6 and TROY regulate brain vascular development. Developmental Cell. 2012; 22:403–417. [PubMed: 22340501]
23. Kierdorf K, et al. Microglia emerge from erythromyeloid precursors via Pu.1- and Irf8-dependent pathways. Nature Neuroscience. 2013; 16:273–280. [PubMed: 23334579]
24. Goldie LC, Lucitti JL, Dickinson ME, Hirschi KK. Cell signaling directing the formation and function of hemogenic endothelium during murine embryogenesis. Blood. 2008; 112:3194–3204. [PubMed: 18684862]
25. Wilson CH, et al. The kinetics of ER fusion protein activation in vivo. Oncogene. 2014; 33:4877–4880. [PubMed: 24662815]
26. Palis J, Robertson S, Kennedy M, Wall C, Keller G. Development of erythroid and myeloid progenitors in the yolk sac and embryo proper of the mouse. Development. 1999; 126:5073–5084. [PubMed: 10529424]
27. Alharbi RA, Pettengell R, Pandha HS, Morgan R. The role of HOX genes in normal hematopoiesis and acute leukemia. Leukemia. 2013; 27:1000–1008. [PubMed: 23212154]
28. Toshner M, et al. Transcript analysis reveals a specific HOX signature associated with positional identity of human endothelial cells. PloS One. 2014; 9:e91334. [PubMed: 24651450]
29. Rossig L, et al. Histone deacetylase activity is essential for the expression of HoxA9 and for endothelial commitment of progenitor cells. The Journal of Experimental Medicine. 2005; 201:1825–1835. [PubMed: 15928198]
30. Browning AC, et al. Comparative gene expression profiling of human umbilical vein endothelial cells and ocular vascular endothelial cells. Br J Ophthalmol. 2012; 96:128–132. [PubMed: 22028475]
31. Nonaka H, Tanaka M, Suzuki K, Miyajima A. Development of murine hepatic sinusoidal endothelial cells characterized by the expression of hyaluronan receptors. Developmental Dynamics. 2007; 236:2258–2267. [PubMed: 17626278]
32. Majesky MW. Developmental basis of vascular smooth muscle diversity. Arteriosclerosis, Thrombosis, and Vascular biology. 2007; 27:1248–1258.
33. Liu C, et al. Macrophages Mediate the Repair of Brain Vascular Rupture through Direct Physical Adhesion and Mechanical Traction. Immunity. 2016; 44:1162–1176. [PubMed: 27156384]
34. Goldman O, et al. Endoderm generates endothelial cells during liver development. Stem Cell Reports. 2014; 3:556–565. [PubMed: 25358784]
35. Matsumoto K, Yoshitomi H, Rossant J, Zaret KS. Liver organogenesis promoted by endothelial cells prior to vascular function. Science. 2001; 294:559–563. [PubMed: 11577199]
36. Srinivas S, et al. Cre reporter strains produced by targeted insertion of EYFP and ECFP into the ROSA26 locus. BMC Dev Biol. 2001; 1:4. [PubMed: 11299042]
37. Madisen L, et al. A robust and high-throughput Cre reporting and characterization system for the whole mouse brain. Nature Neuroscience. 2010; 13:133–140. [PubMed: 20023653]
38. Kawamoto S, et al. A novel reporter mouse strain that expresses enhanced green fluorescent protein upon Cre-mediated recombination. FEBS Letters. 2000; 470:263–268. [PubMed: 10745079]

39. McKercher SR, et al. Targeted disruption of the PU.1 gene results in multiple hematopoietic abnormalities. The EMBO Journal. 1996; 15:5647–5658. [PubMed: 8896458]
40. Scott EW, Simon MC, Anastasi J, Singh H. Requirement of transcription factor PU.1 in the development of multiple hematopoietic lineages. Science. 1994; 265:1573–1577. [PubMed: 8079170]
41. Yamazaki T, et al. Tissue Myeloid Progenitors Differentiate into Pericytes through TGF-beta Signaling in Developing Skin Vasculature. Cell Reports. 2017; 18:2991–3004. [PubMed: 28329690]
42. Kmita M, et al. Early developmental arrest of mammalian limbs lacking HoxA/HoxD gene function. Nature. 2005; 435:1113–1116. [PubMed: 15973411]
43. Klein S, et al. Interstitial cells of Cajal integrate excitatory and inhibitory neurotransmission with intestinal slow-wave activity. Nature Communications. 2013; 4
44. Zarkada G, Heinolainen K, Makinen T, Kubota Y, Alitalo K. VEGFR3 does not sustain retinal angiogenesis without VEGFR2. Proceedings of the National Academy of Sciences of the United States of America. 2015; 112:761–766. [PubMed: 25561555]
45. Yoshida H, et al. The murine mutation osteopetrosis is in the coding region of the macrophage colony stimulating factor gene. Nature. 1990; 345:442–444. [PubMed: 2188141]
46. Fantin A, Vieira JM, Plein A, Maden CH, Ruhrberg C. The embryonic mouse hindbrain as a qualitative and quantitative model for studying the molecular and cellular mechanisms of angiogenesis. Nature Protocols. 2013; 8:418–429. [PubMed: 23424750]
47. Gory-Faure S, et al. Role of vascular endothelial-cadherin in vascular morphogenesis. Development. 1999; 126:2093–2102. [PubMed: 10207135]
48. McLaughlin F, Ludbrook VJ, Kola I, Campbell CJ, Randi AM. Characterisation of the tumour necrosis factor (TNF)-(alpha) response elements in the human ICAM-2 promoter. J Cell Sci. 1999; 112(Pt 24):4695–4703. [PubMed: 10574717]
49. Morgan SM, Samulowitz U, Darley L, Simmons DL, Vestweber D. Biochemical characterization and molecular cloning of a novel endothelial-specific sialomucin. Blood. 1999; 93:165–175. [PubMed: 9864158]
50. Albelda SM, Muller WA, Buck CA, Newman PJ. Molecular and cellular properties of PECAM-1 (endoCAM/CD31): a novel vascular cell-cell adhesion molecule. J Cell Biol. 1991; 114:1059–1068. [PubMed: 1874786]
51. Shalaby F, et al. Failure of blood-island formation and vasculogenesis in Flk-1-deficient mice. Nature. 1995; 376:62–66. [PubMed: 7596435]
52. Austyn JM, Gordon S. F4/80, a monoclonal antibody directed specifically against the mouse macrophage. European Journal of Immunology. 1981; 11:805–815. [PubMed: 7308288]
53. Ohsawa K, Imai Y, Sasaki Y, Kohsaka S. Microglia/macrophage-specific protein Iba1 binds to fimbrin and enhances its actin-bundling activity. Journal of Neurochemistry. 2004; 88:844–856. [PubMed: 14756805]
54. Ozerdem U, Grako KA, Dahlin-Huppe K, Monosov E, Stallcup WB. NG2 proteoglycan is expressed exclusively by mural cells during vascular morphogenesis. Developmental Dynamics. 2001; 222:218–227. [PubMed: 11668599]
55. Goodell MA, Brose K, Paradis G, Conner AS, Mulligan RC. Isolation and functional properties of murine hematopoietic stem cells that are replicating in vivo. The Journal of Experimental Medicine. 1996; 183:1797–1806. [PubMed: 8666936]
56. Bolger AM, Lohse M, Usadel B. Trimmomatic: a flexible trimmer for Illumina sequence data. Bioinformatics. 2014; 30:2114–2120. [PubMed: 24695404]
57. Dobin A, et al. STAR: ultrafast universal RNA-seq aligner. Bioinformatics. 2013; 29:15–21. [PubMed: 23104886]
58. Liao Y, Smyth GK, Shi W. featureCounts: an efficient general purpose program for assigning sequence reads to genomic features. Bioinformatics. 2014; 30:923–930. [PubMed: 24227677]
59. Varet H, Brillet-Gueguen L, Coppee JY, Dillies MA. SARTools: A DESeq2- and EdgeR-Based R Pipeline for Comprehensive Differential Analysis of RNA-Seq Data. PloS One. 2016; 11:e0157022. [PubMed: 27280887]

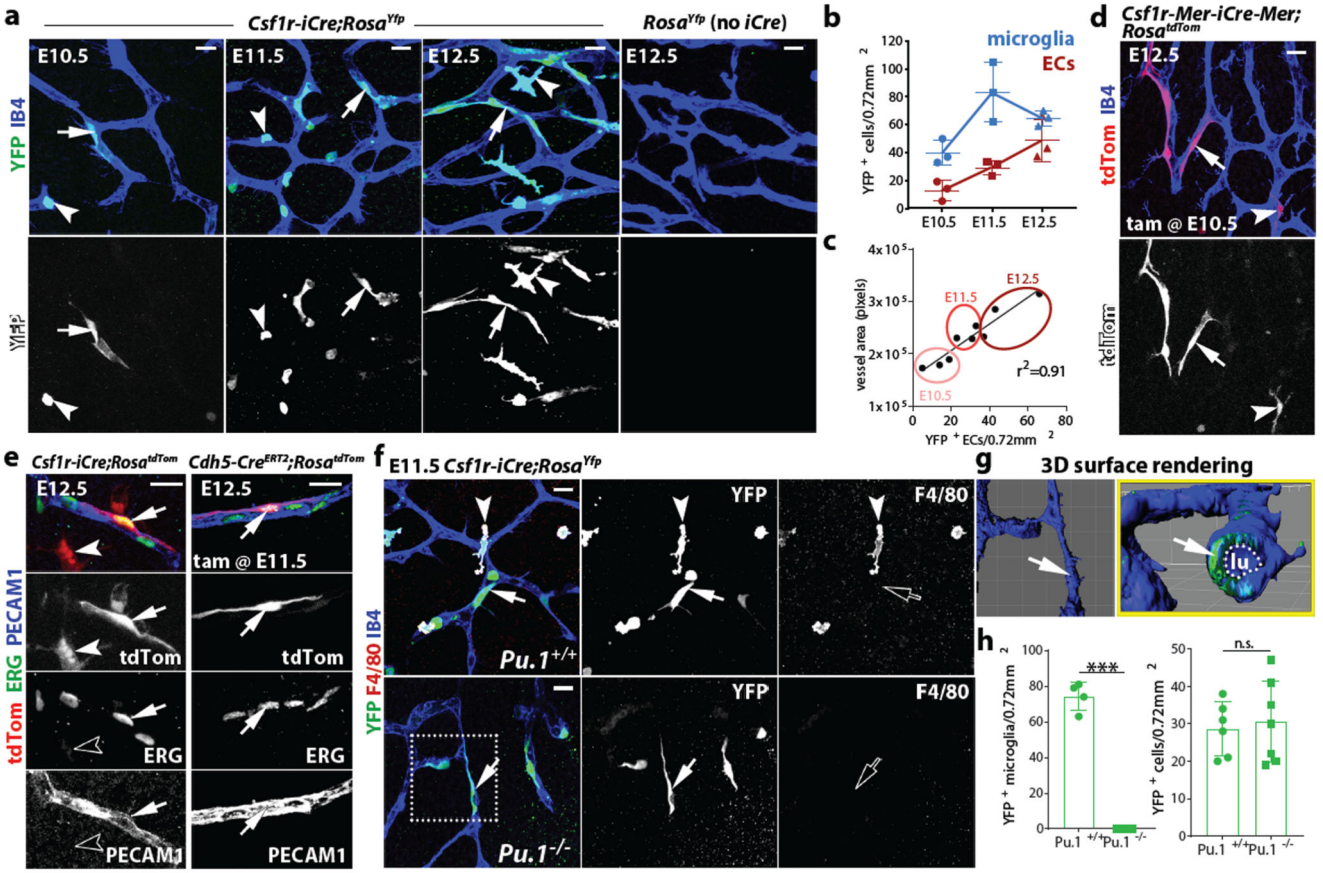

Fig. 1. *Csf1r-iCre* lineage tracing identifies ECs in developing brain vasculature.

(**a-c**) *Csf1r-iCre;Rosa*^{Yfp} hindbrains of the indicated gestational stages. (**a**) Wholemount labelling for YFP and IB4; (**b**) YFP$^+$ IB4$^+$ single cells (microglia) and YFP$^+$ IB4$^+$ vessel-bound cells (putative ECs) per 0.72 mm^2, mean ± SD; (**c**) positive correlation between YFP$^+$ putative EC number and vessel area (r^2, coefficient of determination; goodness of fit, $P < 0.01$); each data point represents one hindbrain, n = 3 hindbrains for each group.

(**d,e**) E12.5 hindbrains of the indicated genotypes, wholemount labelled with the indicated markers and shown including tdTom fluorescence; *Csf1r-Mer-iCre-Mer;Rosa*^{tdTom} (**d**) was tamoxifen-induced on E10.5 and *Cdh5-Cre*^{ERT2}*;Rosa*^{tdTom} (**e**) on E11.5; n = 3 hindbrains for each genotype.

(**f-h**) *Csf1r-iCre;Rosa*^{Yfp} E11.5 hindbrains on a *Pu.1*$^{+/+}$ versus *Pu.1*$^{-/-}$ background, labelled for YFP and F4/80 together with IB4. The boxed area in (**f**) was 3D surface rendered and is shown in (**g**) en face and as a lateral view starting at the plane indicated by the yellow line; the vascular lumen (lu) is outlined. (**h**) YFP$^+$ microglia (*Pu.1*$^{+/+}$ n = 4; *Pu.1*$^{-/-}$ n = 3) and ECs (*Pu.1*$^{+/+}$ n = 6; *Pu.1*$^{-/-}$ n = 7), mean ± SD; each data point represents one hindbrain; n.s., non-significant; ***$P < 0.0001$ (two-tailed unpaired t-test).

Symbols: Microglia and ECs are indicated with arrowheads and arrows, respectively. Solid and clear symbols indicate the presence or absence of marker expression, respectively.

Scale bars: 20 μm (**a,d,f**), 50 μm (**e**).

Europe PMC Funders Author Manuscripts

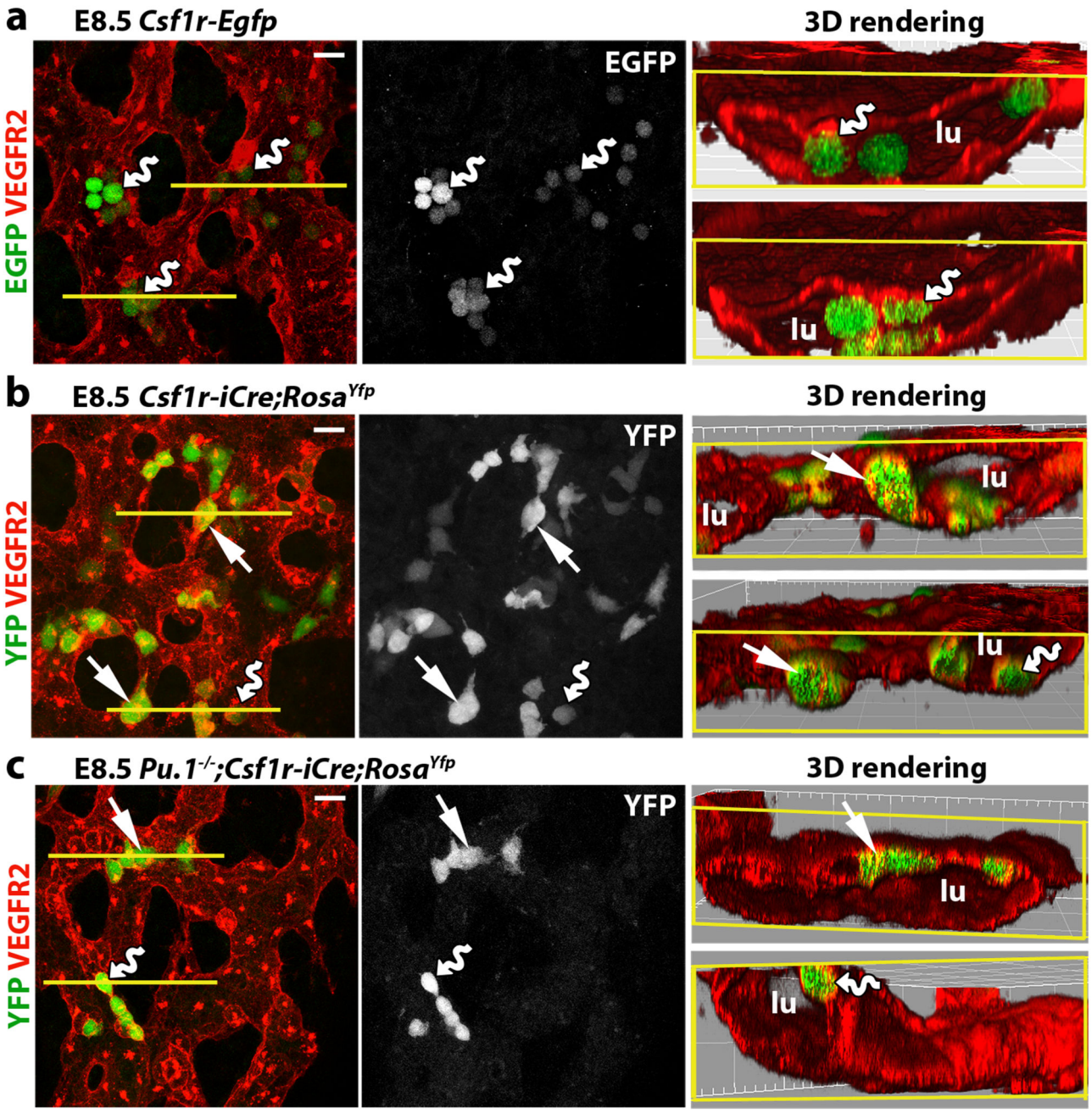

Fig. 2. *Csf1r-iCre*-targeted ECs emerge concomitantly with EMPs in the yolk sac.

E8.5 yolk sacs were wholemount labelled with the indicated markers. (**a**) *Csf1r-Egfp* yolk sacs. (**b,c**) *Csf1r-iCre;Rosa*^{Yfp} yolk sacs on a *Pu.1*$^{+/+}$ versus (**b**) *Pu.1*$^{-/-}$ background (**c**). N = 4 yolk sacs for each genotype. The yellow lines mark the start of 3D-rendered lateral views. Wavy arrows indicate VEGFR2^{+} EGFP^{+} and VEGFR2^{+} YFP^{+} round EMPs/MPs protruding from the vascular wall into the lumen (lu) and straight arrows indicate YFP^{+} VEGFR2^{+} flat cells within the vascular wall. *Scale bars*: 20 μm.

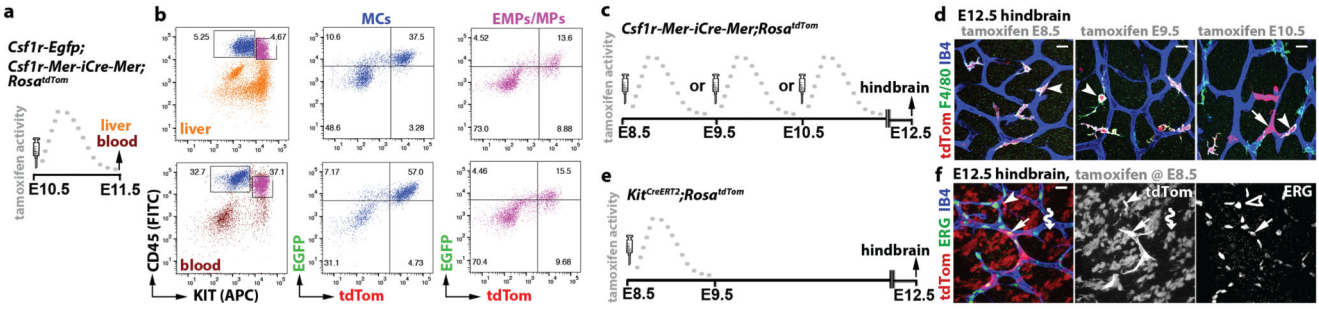

Fig. 3. *Csf1r-iCre*-targeted hindbrain ECs emerge from intraembryonic EMPs.

(**a,b**) A pregnant *Csf1r-Egfp*;*Csf1r-Mer-iCre-Mer;Rosa*^{tdTom} dam was injected with a single tamoxifen dose on E10.5 (**a**) before FACS of E11.5 liver and blood cells (**b**) to gate the CD45^{hi} KIT^{-} differentiated MCs (blue) and CD45^{lo} KIT^{+} EMP/MP populations (pink) for EGFP and tdTom (n = 4 embryos).

(c-f) Pregnant *Csf1r-Mer-iCre-Mer;Rosa*^{tdTom} (**c,d**) and *Kit*$^{CreERT2;}$*Rosa*^{tdTom} (**e,f**) dams were injected with a single tamoxifen dose on the indicated days before E12.5 hindbrain wholemount staining for the indicated markers and imaging including tdTom fluorescence. *Symbols*: Arrows indicate tdTom^{+} ECs, arrowheads macrophages/microglia and the wavy arrow a cluster of tdTom^{+} ERG^{-} IB4^{-} neural cells derived from *Kit*$^{+}$ neural progenitors. *Scale bars*: 20 μm.

Europe PMC Funders Author Manuscripts

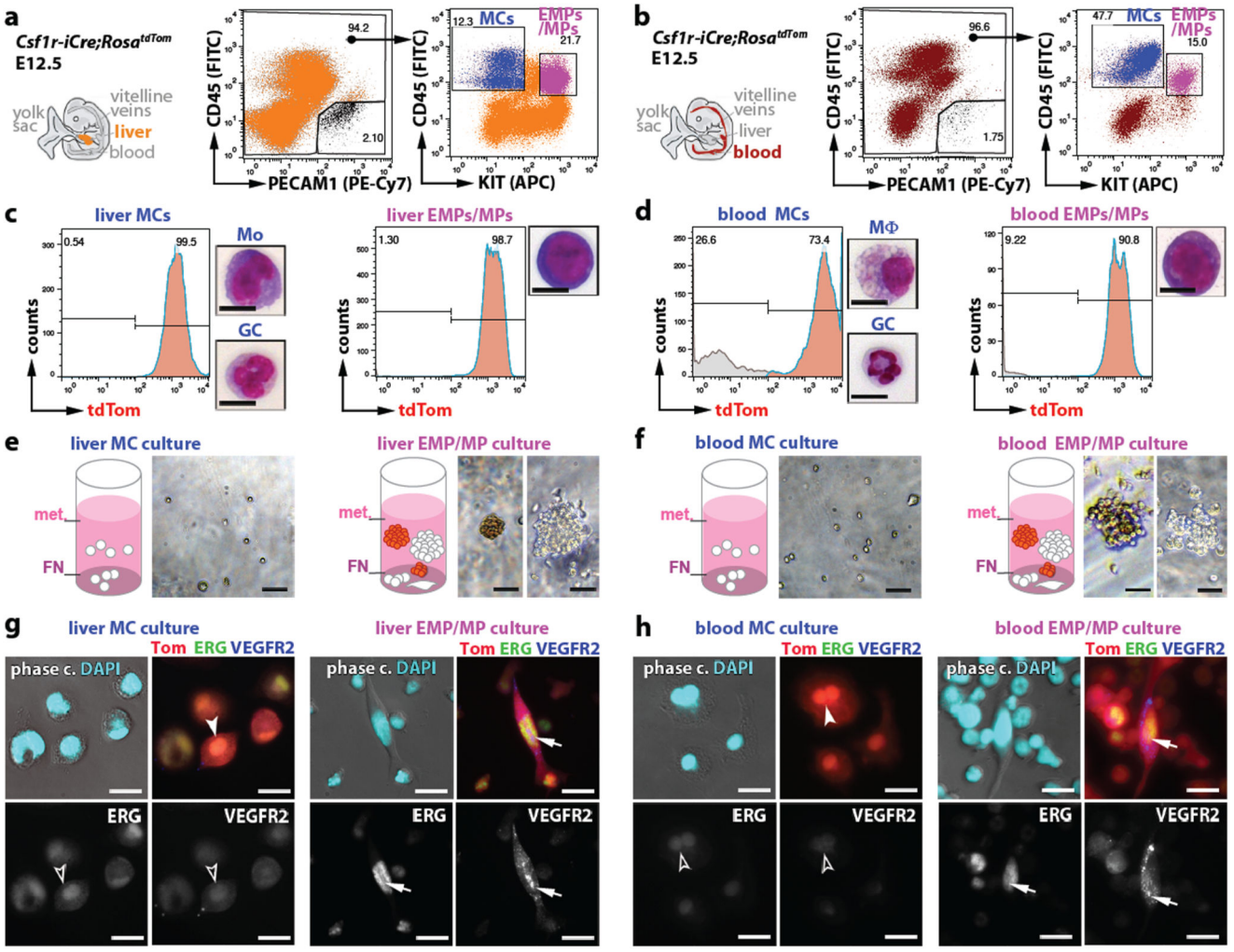

Fig. 4. EMPs in the liver and blood give rise to ECs *in vitro*.

(**a,b**) FACS strategy to separate the differentiated MC and EMP/MP populations from E12.5 *Csf1r-iCre;Rosa*^{tdTom} liver (**a**) and blood (**b**) using antibodies for CD45 and KIT after excluding PECAM1^{+} cells to prevent EC contamination.

(**c,d**) tdTom^{+} proportion in the FACS-isolated MC and EMP/MP populations from liver and blood shown in (**a,b**), and Giemsa-Wright staining of representative cells (Mo, monocyte; GC, granulocyte; Mϕ, macrophage).

(**e-h**) Brightfield images of myeloid (white) and erythroid (rust-coloured) colonies (**e,f**) and immunofluorescence of adherent cells (**g,h**) after three days in methocult (met.) on FN. Adherent cells were immunolabelled for ERG and VEGFR2, counterstained with DAPI and are shown together with tdTom fluorescence (Tom). *Symbols*: Arrows indicate tdTom^{+} ECs, arrowheads tdTom^{+} MCs; solid and clear symbols indicate high versus low marker expression, respectively. *Scale bars*: 20 μm.

N=3 independent experiments.

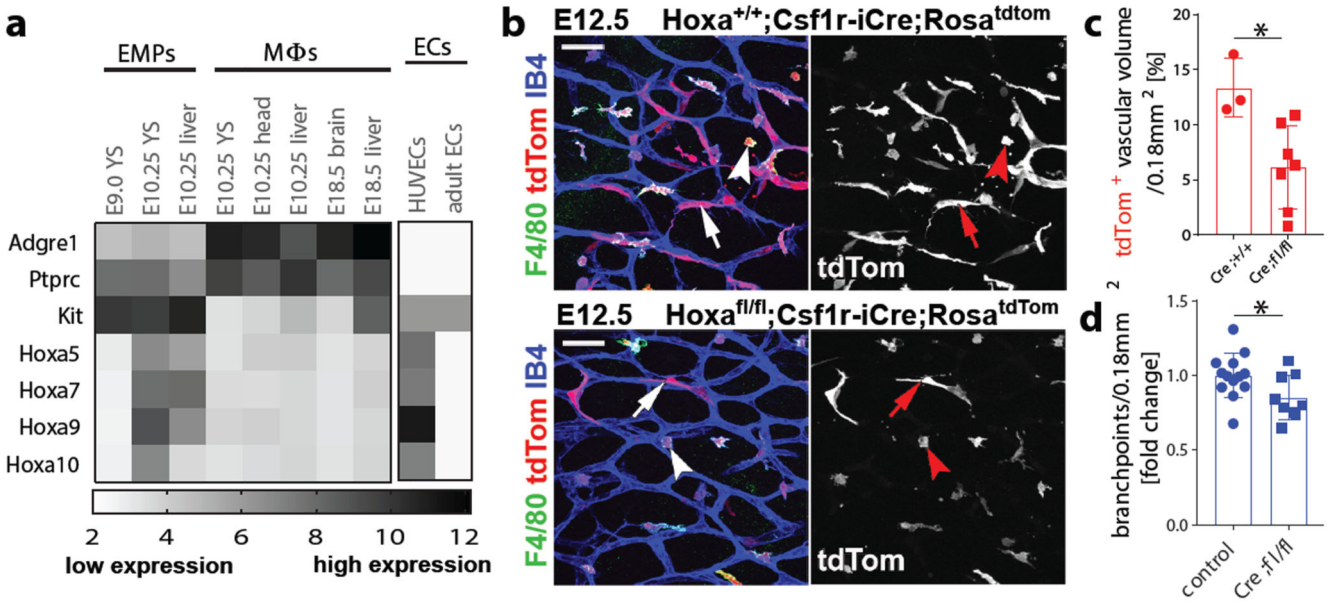

Fig. 5. *Csf1r-iCre*-targeted ECs form in a *Hoxa*-dependent mechanism and promote vascularisation in the embryonic hindbrain.

(**a**) Transcriptomic analysis of the indicated cell populations for the indicated genes, based on published RNAseq (n = 2, except for E10.25 YS (4) and head (3) Mϕs) 9, 30 and EC microarray data (n = 3) 9, 30, shows that *Hoxa* transcripts are enriched in intraembryonic EMPs*;* white and black represent low versus high relative expression; Mϕs, macrophages; YS, yolk sac; HUVECs, human umbilical cord ECs; *Adgre1* and *Ptprc*, encode F4/80 and CD45, respectively.

(**b-d**) E12.5 littermate hindbrains of the indicated genotypes. (**b**) Wholemount labelling for the indicated markers; RFP staining to visualise tdTom demonstrates fewer *Csf1r-iCre*-targeted ECs; s*ymbols*: arrows and arrowheads indicate $tdTom^+$ ECs and microglia, respectively; s*cale bars*: 50 μm. (**c**) $tdTom^+$ relative to $IB4^+$ EC volume in $Hoxa^{+/+}$ (n = 3) versus $Hoxa^{fl/fl}$ (n = 7) hindbrains on a $Csf1r\text{-}iCre;Rosa^{tdTom}$ background, mean ± SD. (**d**) SVP complexity, measured as fold change of vascular branchpoints in $Hoxa^{fl/fl};Csf1r\text{-}iCre$ (n = 9) relative to control (pooled $Csf1r\text{-}iCre^{+};Hoxa^{+/+}$ and $Csf1r\text{-}iCre^{-}$ of any *Hoxa* genotype, n = 13) hindbrains, mean ± SD. Each data point represents one hindbrain; *P = 0.0184 (**c**), *P = 0.0323 (**d**) (two-tailed unpaired t-test).

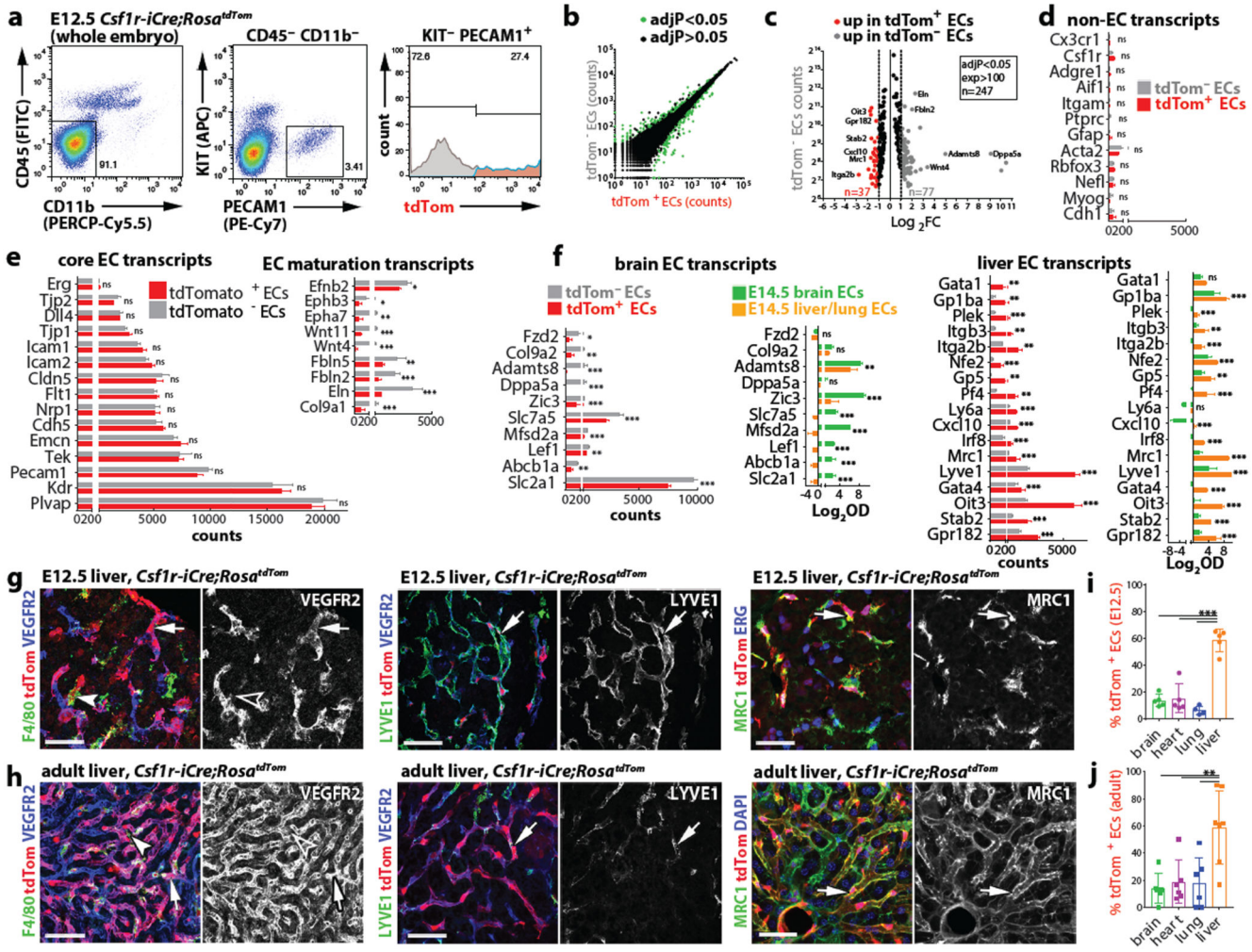

Fig. 6. The *Csf1r-iCre*-targeted EC population has a core endothelial transcription signature with an increase in liver EC transcripts and persists in adult organs.

(**a-f**) Transcriptomic analysis. (**a**) FACS strategy to isolate tdTom^{-} and tdTom^{+} ECs from E12.5 *Csf1r-iCre;Rosa*^{tdTom} embryos for RNA-Seq. (**b**) Graphic representation of genes whose expression is significantly different (green dots) and similar (black dots) between both EC populations. (**c**) Volcano plot of significantly differentially expressed transcripts with > 100 counts per transcript; selected genes are named; grey and red data points represent transcripts in tdTom^{-} ECs with ≥ 2-fold over- or under-representation, respectively. Relative expression levels for: (**d**) markers typical of myeloid (*Cx3cr1-Ptprc*), astrocytic (*Gfap*), smooth muscle (*Acta2*), neuronal (*Rbfox3*, *Nefl*), skeletal muscle (*Myog*) or epithelial (*Cdh1*) differentiation; (**e**) EC core and maturation markers; (**f**) representative brain and liver EC specialisation markers, shown alongside their relative expression in brain versus liver/lung ECs microarrays 30. Mean ± SD; RNA-Seq, n = 3 embryos (DESeq2; Benjamini-Hochberg's multiple comparisons test for p-value adjustment, adjP); microarray, n = 5 organs (2-way ANOVA, Bonferroni's multiple comparisons test); ns, non-significant, *P < 0.05, **P < 0.01, ***P < 0.0001; see Source Data Figure 6 for exact values.

Europe PMC Funders Author Manuscripts

(**g,h**) *Csf1r-iCre;Rosa*^{tdTom} E12.5 (**g**) and adult (**h**) liver cryosections, labelled for the indicated markers and RFP to visualise tdTom, including DAPI counterstaining in (**h**); n = 3 independent experiments. *Symbols*: Arrows and arrowheads indicate tdTom^{+} ECs and macrophages, respectively; clear arrowheads indicate that macrophages lack VEGFR2. *Scale bar*: 50 μm.

(**i,j**) FACS of *Csf1r-iCre;Rosa*^{tdTom} E12.5 (**i**) and adult (**j**) brain, heart, lung and liver to determine their relative tdTom^{+} EC contribution; mean ± SD; n = 5 organs each (**i**; except lung, n = 4), n = 6 organs each (**j**; except liver, n = 7); each data point represents one organ; ***P < 0.0001 (**i**); **P = 0.0023, 0.0066, 0.00541 (**j**) for liver versus brain, heart, lung, respectively (1-way ANOVA, Tukey's multiple comparisons test).

Europe PMC Funders Author Manuscripts